Spin−Orbit Coupling in the Oxidative Activation of H−H by FeO^+. Selection Rules and Reactivity Effects

David Danovich and Sason Shaik*,†

Contribution from The Institute of Chemistry and The Minerva Center of Computational Quantum Chemistry, The Hebrew University, 91904 Jerusalem, Israel

Received August 28, 1996. Revised Manuscript Received December 10, 1996[⊗]

Abstract: Spin−orbit coupling (SOC) calculations are performed along the reaction pathway of the oxidation process, $FeO^+ + H_2 \rightarrow Fe^+ + H_2O$ (eq 1). Selection rules are derived for SOC between different spin situations, and are applied to understand the computed SOC patterns along the oxidation pathway, and their relationship to the electronic structure of the various species. The process involves two spin inversion (SI) junctions between sextet and quartet states: near the FeO^+/H_2 cluster at the entrance channel, and near the Fe^+/H_2O cluster at the exit channel. The sextet−quartet SOC is significant at the reactant extreme (for FeO^+), but decreases at the FeO^+/H_2 cluster and continues to decrease until it becomes vanishingly small between the $^6D-^4F$ states of Fe^+ at the product extreme. The results show that while the quartet surface provides a low-energy path, the SI junctions reduce the probability of the oxidation process significantly. In agreement with the deductions of Armentrout et al.,[2c] the poor bond activation capability of the ^6D ground state of Fe^+ in the reverse reaction is accounted for by the inefficient $^6D-^4F$ state mixing due to the expected poor SOC between the respective $4s^13d^6$ and $3d^7$ configurations. On the other hand, the ^4F excited state of Fe^+ can activate H_2O more efficiently since it can lead to the insertion intermediate $^4(HFeOH^+)$ in a spin-conserving manner. Other findings of Schwarz et al.[1,2a] and Armentrout et al.[2c,d] are discussed in the light of the SOC patterns. The importance of the SOC at the exit channel is highlighted by comparing the product distribution of the reaction (eq 1) with analogous reactions of MO^+ species: when the ground state M^+ has a $4s^13d^{n-1}$ (Fe^+, Mn^+) electronic structure as opposed to those cases where the ground state electronic structure is $3d^n$ (Co^+, Ni^+) and where no spin inversion is required. Predictions based on the understanding of the SOC patterns are made and compared with appropriate experimental data.

Introduction

Gas-phase C−H/C−C bond activation by "bare" oxo-transition-metal cations (MO^+)[1] has generated intriguing patterns[2] which seem to reflect the interplay of classical factors, e.g., barrier heights with spin-inversion (SI) bottlenecks due to the crossing of surfaces of different spin multiplicities.[3] A typical example is the oxidation of H_2 by FeO^+ ($^6\Sigma^+$) in eq 1, which has been studied mechanistically by the Berlin[2a] and Utah[2c] groups. Despite the high exothermicity of the process ($\Delta H = -36$ kcal/mol), its seemingly spin-conserving nature, and the absence of any unusual orbital restrictions, the process is nonetheless inefficient and occurs only once in every 100−1000 collisions.[1,2a,c] The reactions of CoO^+ and NiO^+ which are more exothermic are even less efficient.[2b,d]

$$FeO^+(^6\Sigma^+) + H_2 \rightarrow Fe^+(^6D) + H_2O \qquad (1)$$

Figure 1, which shows schematically the potential energy curves[2e,c] for the reaction, reveals a possible origin of the problem. The reaction starts at the reactant (R) entrance channel on a surface with a sextet spin multiplicity and changes over to a quartet insertion intermediate, ^4I ($HFeOH^+$). Since the ground state of the Fe^+ product is ^6D, another SI junction exists at the exit stage of the reaction. As such, the transformation in eq 1 exhibits a two-state reactivity having both barriers and SI junctions along the way.[2c,e,3,4] Thus, on the one hand, *the quartet*

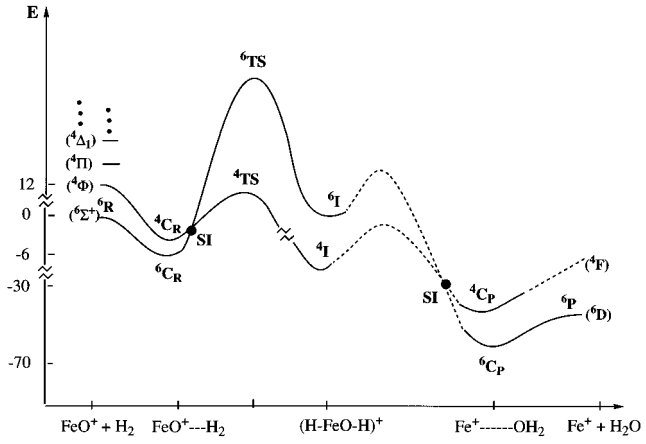

Figure 1. A schematic potenial energy profile for the reaction in eq 1. For computational details of energies (in kcal/mol) and structures see refs 2e and 21. The dashed lines indicate areas unexplored computationally.

† All correspondence should be addressed to S.S. at the Department of Organic Chemistry, The Hebrew University, 91904 Jerusalem, Israel. E-mail: sason@yfaat.ch.huji.ac.il. FAX: +972-2-6585345.

⊗ Abstract published in *Advance ACS Abstracts,* February 1, 1997.

(1) For a recent review see: Schröder, D.; Schwarz, H. *Angew. Chem., Int. Ed. Engl.* **1995**, *34*, 1973.

(2) (a) Schröder, D.; Fiedler, A.; Ryan, M. F.; Schwarz, H. *J. Phys. Chem.* **1994**, *98*, 68. (b) Ryan, M. F.; Fiedler, A.; Schröder, D.; Schwarz, H. *Organometallics* **1994**, *13*, 4072. (c) Clemmer, D. E.; Chen, Y.-M.; Khan, F. A.; Armentrout, P. B. *J. Phys. Chem.* **1994**, *98*, 6522. (d) Chen, Y.-M.; Clemmer, D. E.; Armentrout, P. B. *J. Am. Chem. Soc.* **1994**, *116*, 7815. (e) Fiedler, A.; Schröder, D.; Shaik, S.; Schwarz, H. *J. Am. Chem. Soc.* **1994**, *116*, 10734. (f) Irikura, K. K.; Beauchamp, J. L. *J. Am. Chem. Soc.* **1986**, *108*, 7502. (g) Schröder, D.; Schwarz, H. *Angew. Chem., Int. Ed. Engl.* **1991**, *30*, 820. Schröder, D.; Fiedler, A.; Hrusak, J.; Schwarz, H. *J. Am. Chem. Soc.* **1992**, *114*, 1215.

(3) Shaik, S.; Danovich, D.; Fiedler, A.; Schröder, D.; Schwarz, H. *Helv. Chim. Acta* **1995**, *78*, 1393.

(4) (a) Armentrout, P. B. *Science* **1991**, *251*, 175. (b) Elkind, J. L.; Armentrout, P. B. *J. Phys. Chem.* **1986**, *90*, 5736. (c) Fisher, E. R.; Schultz, R. H.; Armentrout, P. B. *J. Phys. Chem.* **1989**, *93*, 7382. (d) Schultz, R. H.; Elkind, J. L.; Armentrout, P. B. *J. Am. Chem. Soc.* **1988**, *110*, 411. (e) Aristov, N.; Armentrout, P. B. *J. Am. Chem. Soc.* **1986**, *108*, 1806.

S0002-7863(96)03033-8 CCC: $14.00

surface provides a low-energy path which enables bond activation, but on the other hand the poor efficiency of the reaction may well originate in the probability to cross the SI junctions.

The pioneering studies of Armentrout et al.[2d,4] have emphasized that a necessary condition for an efficient reaction like eq 1 is that the MO^+ species will possess a suitable electronic structure which permits a spin-allowed (spin-conserving) reaction. The reactivity consequences of spin conservation have been demonstrated by elegant studies of Armentrout et al.[4] and Weisshaar et al.,[5] who showed that C−C/C−H bond activation by metal cations, M^+, is *state selective* and proceeds much more efficiently from those M^+ states which can form the insertion intermediates RMH^+ in a spin-conserving manner. Thus, the ^{6}D ground state of Fe^+ reacts sluggishly with RH species, in comparison with the lower-spin excited state, $Fe^+(^4F)$, which correlates efficiently in a spin-conserving manner to the insertion intermediates $^4(RMH^+)$. Similar differences are observed for bond activation by V^+ for which the low-spin ^{3}F excited state is 270 more efficient toward ethane than the ^{5}D ground state.[4e,5e] Further, it has been concluded[4e,5d,e] that the exalted bond activating capability of the low-spin excited states is not associated with the excess energy of the excited state[5d] but rather with its spin multiplicity match with the insertion intermediate. These results imply therefore that the spin conservation is a crucial ingredient in C−H and H−H activation by first-row transition-metal species.

This interplay of reactivity factors may be generally expected for reactions of coordinatively unsaturated transition-metal compounds which often possess high-spin ground states and nearby low-spin excited states.[6] As a result of the state adjacency and the better bonding capability of the low-spin states, the different spin states intersect[3,4a,5e] and generate SI junctions. Indeed the reactivity of coordinatively unsaturated ML_n species and bare metal ions[7] is marked by crossings of different spin situations. For example, recent calculations[7b] show that in the reaction of Fe^+ with C_2H_6 there exists an SI junction at the entrance channel (formation of clusters), while barriers at the exit channel dominate and thereby affect the product distribution. Therefore, to conceptualize reactivity patterns as a whole, it is essential to achieve understanding of factors which affect the passage of such SI junctions, between different spin situations.

Whether a SI junction may or may not act as a bottleneck depends, *inter alia*, on the degree of mixing of the spin situations which intend to cross. The principal mechanism which mixes the two spin states and provides probability of crossover of the SI junction is spin−orbit coupling (SOC).[8] As such, the knowledge of SOC as a function of structure is a prerequisite to the understanding of the potential role of SI. Despite the important qualitative understanding of SOC patterns in singlet−triplet[9] and in a variety of other spin situations,[10] the topic as a whole remains among the least understood chemical effects. Consequently, the principal aim of the present paper is to establish guidelines and qualitative rules necessary to understand the SOC patterns *between different spin situations*, as a function of geometry and electronic structure. This will be attempted by combining a detailed quantum chemical calculation of SOC factors along with a qualitative analysis of these factors in the activation of H_2 by FeO^+ described in eq 1.

The first part of the paper describes the computational results of SOC factors for a few critical species on the reaction pathway of Figure 1. These results are obtained by use of the one-electron method[11a,b] which has been applied successfully to main elements as well as to heavy transition metal species.[11c] The second part of the paper derives the selection rules needed for the analysis of the computational trends. Our approach relies on the phenomenological SOC Hamiltonian[8a,b] compatible with the approximate expression in eq 2. As such, our analysis draws on and has complementary aspects to the general treatment of SOC by Lefebvre-Brion and Field[8a] and the work of Peyerimhoff et al.[10a] Finally, the SOC matrix elements will form a basis for a discussion of the possible role of the SI junction in the overall poor efficiency of the bond activation process in eq 1.

Methods

Treatments of SOC involving the full Breit-Pauli Hamiltonian have been developed by several groups[9e−g,10a−k] and applied to diatomic

(5) (a) Hanton, S. D.; Noll, R. J.; Weisshaar, J. C. *J. Phys. Chem.* **1990**, *94*, 5655. (b) Sanders, L.; Hanton, S. D.; Weisshaar, J. C. *J. Phys. Chem.* **1987**, *91*, 5145. (c) Sanders, L.; Hanton, S. D.; Weisshaar, J. C. *J. Phys. Chem.* **1989**, *93*, 1963. (d) Sanders, L.; Hanton, S. D.; Weisshaar, J. C. *J. Phys. Chem.* **1990**, *92*, 3498. (e) Weisshaar, J. C. *Acc. Chem. Res.* **1993**, *26*, 213. (f) Tonkyn, R.; Weisshaar, J. C. *J. Phys. Chem.* **1986**, *90*, 2305. Tonkyn, R.; Ronan, M.; Weisshaar, J. C. *J. Phys. Chem.* **1988**, *92*, 92.

(6) (a) Koga, N.; Morokuma, K. *Chem. Rev.* **1991**, *91*, 823. (b) Widmark, P. D.; Roos, B. O.; Seigbahn, P. E. *J. Phys. Chem.* **1985**, *89*, 2180. (c) Carter, E. A.; Goddard, W. A. *J. Phys. Chem.* **1988**, *92*, 5679. (d) Ohanessian, G.; Goddard, W. A., III *Acc. Chem. Res.* **1990**, *23*, 386.

(7) (a) Heinemann, C.; Goldberg, N.; Tornieporth-Oettig, I. C.; Klaptöke, T. M.; Schwarz, H. *Angew. Chem., Int. Ed. Engl.* **1995**, *34*, 213. (b) Holthausen, M. C.; Fiedler, A.; Schwarz, H.; Koch, W. *Angew. Chem., Int. Ed. Engl.* **1995**, *34*, 2282. Holthausen, M. C.; Fiedler, A.; Schwarz, H.; Koch, W. *J. Phys. Chem.* **1996**, *100*, 6236. (c) Schröder, D.; Fiedler, A.; Wolfgang, A.; Herrmann, W. A.; Schwarz, H. *Angew. Chem., Int. Ed. Engl.* **1995**, *34*, 2517. (d) Perry, J. K.; Ohanessian, G.; Goddard, W. A., III *Organometallics* **1994**, *13*, 1870. (e) Musaev, D. G.; Morokuma, K. *Isr. J. Chem.* **1993**, *33*, 307. (f) Rappé, A. K.; Upton, T. H. *J. Chem. Phys.* **1986**, *85*, 4400. (g) Cornhell, H. H.; Heinemann, C.; Schröder, D.; Schwarz, H. *Organometallics* **1995**, *14*, 992.

(8) General sources for discussions of SOC are the following: (a) Lefebvre-Brion, H.; Field, R. W. *Perturbations in the Spectra of Diatomic Molecules*; Academic Press: New York, 1986. (b) McGlynn, S. P.; Azumi, T.; Kinoshita, M. *Molecular Spectroscopy of the Triplet State*; Prentice-Hall: Englewood-Cliffs, NJ, 1969. (c) Matsen, F. A.; Klein, D. J. *Adv. Photochem.* **1969**, *7*, 1. (d) Richards, W. G.; Trivedi, H. P.; Cooper, D. L. *Spin−Orbit Coupling in Molecules*; Clarendon Press: Oxford, 1981. (e) Ross, R. B.; Christiansen, R. A. *Adv. Quantum Chem.* **1988**, *19*, 139.

(9) For discussions and computations of SOC patterns in singlet−triplet situations, see: (a) Salem, L.; Rowland, C. *Angew. Chem., Int. Ed. Engl.* **1972**, *11*, 92. (b) Michl, J. *J. Am. Chem. Soc.* **1996**, *118*, 3568. (c) Shaik, S. S.; Epiotis, N. D. *J. Am. Chem. Soc.* **1978**, *100*, 18. Shaik, S. S. *J. Am. Chem. Soc.* **1979**, *101*, 2736. Shaik, S. S. *J. Am. Chem. Soc.* **1979**, *101*, 3184. Shaik, S. S.; Epiotis, N. D. *J. Am. Chem. Soc.* **1980**, *102*, 122. Larson, J. R.; Epiotis, N. D.; McMurchie, L. E.; Shaik, S. S. *J. Org. Chem.* **1980**, *45*, 1388. (d) Su, Ming-Der *J. Phys. Chem.* **1996**, *100*, 4339. (e) Carlacci, L.; Doubleday, C.; Fourlani, T. R.; King, H. F.; McIver, J. W., Jr. *J. Am. Chem. Soc.* **1987**, *109*, 5323. King, H. F.; Furlani, T. R. *J. Comput. Chem.* **1988**, *9*, 771. Caldwell, R. A.; Carlacci, L.; Doubleday, C.; Furlani, T. R.; King, H. F.; McIver, J. W., Jr. *J. Am. Chem. Soc.* **1988**, *110*, 6901. (f) Morita, A.; Kato, S. *J. Phys. Chem.* **1992**, *96*, 1067. (g) Morita, A.; Kato, S. *J. Phys. Chem.* **1993**, *97*, 3298. (h) Amatatsu, Y.; Morokuma, M.; Yabushita, S. *J. Chem. Phys.* **1991**, *94*, 4858. (i) Zimmerman, H. E.; Kutateladze, A. G.; Maekawa, Y.; Mangette, J. E. *J. Am. Chem. Soc.* **1994**, *116*, 9795. Zimmerman, H. E.; Kutateladze, A. G. *J. Org. Chem.* **1995**, *60*, 6008. Zimmerman, H. E.; Kutateladze, A. G. *J. Am. Chem. Soc.* **1996**, *118*, 249. (j) Lower, K. S.; El-Sayed, M. A. *Chem. Rev.* **1966**, *66*, 199. El-Sayed, M. A. *J. Chem. Phys.* **1963**, *38*, 2834.

(10) For discussions and computations of SOC patterns in a variety of spin situations in transition metal and main element species, see: (a) Hippe, D.; Peyerimhoff, S. D. *J. Chem. Phys.* **1992**, *96*, 3503. (b) de Vivie, R.; Peyerimhoff, S. D. *J. Chem. Phys.* **1989**, *90*, 3660. (c) de Vivie, R.; Peyerimhoff, S. D. *J. Chem. Phys.* **1988**, *89*, 3028. (d) Klotz, R.; Peyerimhoff, S. D. *Mol. Phys.* **1986**, *57*, 573. (e) Matsushita, T.; Klotz, R.; Marian, C. M.; Peyerimhoff, S. D. *Mol. Phys.* **1987**, *62*, 1385. (f) Thümmel, H.; Klotz, R.; Peyerimhoff, S. D. *Chem. Phys.* **1989**, *135*, 229. (g) Peric, M.; Reuter, W.; Peyerimhoff, S. D. *J. Mol. Spectrosc.* **1991**, *148*, 201. (h) de Vivie, R.; Marian, C. M.; Peyerimhoff, S. D. *Chem. Phys.* **1987**, *112*, 349. (i) Yarkony, D. R. *J. Am. Chem. Soc.* **1992**, *114*, 5406. (j) Manna, M. R.; Yarkony, D. R. *J. Chem. Phys.* **1991**, *95*, 1808. (k) Manna, M. R.; Yarkony, D. R. *Chem. Phys. Lett.* **1992**, *188*, 352. (l) Amatatsu, Y.; Yabushita, S.; Morokuma, M. *J. Chem. Phys.* **1994**, *100*, 4894. Yabushita, S.; Morokuma, M. *Chem. Phys. Lett.* **1990**, *175*, 518.

(11) (a) Koseki, S.; Schmidt, M. W.; Gordon, M. S. *J. Phys. Chem.* **1992**, *96*, 10768. (b) Koseki, S.; Gordon, M. S.; Schmidt, M. W.; Matsunaga, N. *J. Phys. Chem.* **1995**, *99*, 12764. (c) Heinemann, C.; Koch, W.; Schwarz, H. *Chem. Phys. Lett.* **1995**, *245*, 509.

molecules, radicals, and diradicals. The CPU consumption of these calculations is often high. To circumvent the problem, Koseki, Schmidt, and Gordon[11a,b] have implemented a semiempirical procedure which relies on the one-electron part[8] of the spin−orbit Hamiltonian, $\mathbf{H}_{SO}$ in eq 2,

$$\mathbf{H}_{SO} = (\alpha^2/2)\sum_i\sum_K (Z_K^*/R_{iK}^3)\mathbf{L}_{iK}\cdot\mathbf{S}_i; \qquad \alpha^2/2 = (e^2/2m_e^2c^2) \quad (2)$$

where $\mathbf{L}_{iK}$ and $\mathbf{S}_i$ are the orbital and spin angular momentum operators for an electron (i) in the framework of the nuclei, indexed by K. To account for the missing two-electron part of the Hamiltonian, the nuclear charge Z_K is replaced by an effective parameter, Z_K^*, which can be taken as the screened nuclear charge.[8a]

The effective $\mathbf{H}_{SO}$ operator is used in this study to calculate SOC matrix elements between pairs of zero-order spin states which corresponds to the sextet and quartet spin situations which cross over in Figure 1. The spin states are themselves described by MCSCF wave functions of the FORS (full optimized reaction space)[12] type. This method is implemented in the GAMESS suite of programs[13] which has been utilized throughout this study. The MCSCF wave functions for the sextet and quartet states of FeO^+ and $[Fe,O,H_2]^+$ species involve an active space of 13 electrons in 11 orbitals; the latter include the valence 4s and 3d orbitals of Fe, the 2s and 2p orbitals of O, and the 1s orbital of H.

For Fe we use an all-electron basis set [8s 4p 2d] contracted from the primitive (14s 9p 5d) basis set of Wachters.[14] This basis set was supplemented with one set of p ($\alpha = 0.115$) and one set of d ($\alpha = 0.1133$) diffuse functions. For oxygen and hydrogen we used respectively the Dunning-Hay[15] double-ζ basis set [4s 2p]/(9s 5p) and (4s)/[2s] based on the primitive sets of Huzinaga.[16]

Calibration of the SOC Constant for Fe$^+$. To test the method against some experimental situation, we applied it to the ^{6}D ground state of Fe^+, where the SOC is a diagonal matrix element within the space of the 30 spin−orbit substates[8a] nascent from five spatially degenerate $4s^13d^6$ configurations.[17a] The resulting multiplet splitting matches the expected Landé interval splitting pattern.[8d] Employing the actual nuclear charge, $Z = 26$, the SOC Hamiltonian leads to a splitting which is 1.844 times the experimental value,[18] and an Fe^+ atomic constant of $\sim$750 cm^{-1}, larger than the accepted value[19] of 416 cm^{-1}. This is anticipated from the analysis of Koseki, Schmidt, and Gordon[11a,b] of the effect of the nuclear charge on SOC parameters. Using $Z^* = Z/1.844$ gives an accurate value of the total SOC splitting 977.35 cm^{-1} and an atomic constant of 407.23 cm^{-1} by construction in accord with the experimental[18,19] values of 977.03 and 416 cm^{-1}, respectively. The intervals between the J levels are, in cm^{-1}, 366.51 (384.77), 285.06 (282.87), 203.6 (194.99), and 122.17 (114.40); the parenthetical values are the experimental intervals. The agreement is seen to be good albeit not perfect, likely because the experimental multiplet is distorted slightly by second-order SOC. The same Z^* reproduces the multiplet splitting of the ^{4}D ($4s^13d^6$) and ^{4}F ($3d^7$) states of Fe^+, within the errors expected from distortions of the experimental multiplets by second-order SOC. It is important to note that the state averaging leads to a ^{4}F state which is too high in energy compared with experiment (the experimental energy gap relative to ^{6}D is 0.25 eV while the computed gap is 1.8 eV). The ^{4}D state's energy on the other hand is properly handled (the experimental energy gap relative to ^{6}D is 1.0 eV while the computed gap is 1.2 eV). The energy discrepancy, however, does not affect the SOC matrix elements. The Z^* values of Fe and O (see ref 11a for Z^*(O)) were used in all subsequent calculations.

The study of the remaining $[Fe,O,H_2]^+$ species focuses on the evaluation of off-diagonal matrix elements between the spatially different spin situations, sextet and quartet, which occur at the SI junctions in Figure 1. The MCSCF routine is able to handle only Abelian point groups, and therefore it was necessary to carry out the calculations for $FeO^+(C_{\infty v})$ at the C_{2v} point group. In the $C_{\infty v}$ point group, the states of FeO^+ involve occupation in π and δ orbitals (see Figure 2 later) which are eigenfunctions of the angular momentum, l_z, operator and are given by the complex linear combinations of the corresponding Cartesian orbitals. As such, each angular momentum state, with the exception of the high-spin state $^6\Sigma^+$, gives rise to two species of different symmetries[10a,d,e] in C_{2v}. For example, both the $^4\Phi$ and $^4\Pi$ states of FeO^+ transform in C_{2v} into combinations of $^4B_1$ and $^4B_2$ (see Figure 2 later) species. Consequently, some state contamination may lead to erroneous SOC results, due to mixing of CSF's of different angular momentum species. To avoid this, we used a very tight convergence criterion to obtain an accurate wave function.[17b] To eliminate further pitfalls, the computations were carried out both at the C_{2v} as well as at the C_s point groups, so that the SOC matrix element is double checked. In each point group, it was also ascertained that the two symmetry species nascent from a given angular momentum state (e.g., $^4B_1$ and $^4B_2$ or $^4A'$ and $^4A''$ for the angular momentum $^4\Pi$ state) possess the exact same energy and SOC matrix element with the $^6A_1$ ($^6A'$) sextet state. This extra caution is required to ensure that the SOC results for the various critical species in Figure 1 are not consequences of errors in the wave function.

The orbital averaging procedure[17a] was utilized also for the $Fe^+\cdots(OH_2)$ cluster in which the Fe^+ orbitals are only slightly perturbed. For all other species in the study, the state averaging produced small SOC matrix elements, while when the optimized orbitals of the lowest state were used for the SOC evaluation the resulting matrix elements were somewhat larger. We therefore report only these latter matrix elements, so that our SI probabilities are overestimated somewhat.

When optimized orbitals were used to evaluate SOC matrix elements, the calculations involve the following three steps: (i) An ROHF calculation is performed for each spin species, at the geometries corresponding to the critical points in Figure 1 (geometries in Scheme 1). (ii) The ROHF orbitals are used then to generate the MCSCF wave function of the appropriate symmetry. (iii) The SOC calculation is performed between pairs of CI wave functions: one belonging to the sextet state and the other to the quartet state. Since the SOC calculation requires a common set of core orbitals, the orbitals of the lowest spin state (from full optimized reaction space (FORS) MCSCF calculation) were used to generate both spin states for the SOC calculation. The same procedure was used for evaluating SOC in the atomic situations with the exception of the cases which involve the ^{4}F state (Tables 3 and 4). In the latter cases, the core orbitals of ^{4}F were replaced with those of ^{6}D, and the active orbitals were reoptimized. The ^{6}D−^{4}F SOC involved therefore two sets of orbitals which differ in their active part.

Identification of the symmetry species associated with a given angular momentum state relied on the projection procedure used by Hiberty and Leforestier[20] to obtain VB determinants from MO

(12) Ruedenberg, K.; Schmidt, M. W.; Gilbert, M. M.; Elbert, S. T. *Chem. Phys.* **1982**, *71*, 51.

(13) GAMESS-USA, Revision Feb. 1995; Schmidt, M. W.; Baldridge, K. K.; Boatz, J. A.; Elbert, S. T.; Gordon, M. S.; Jensen, J. H.; Koseki, S.; Matsunaga, N.; Nguyen, K. A.; Su, S. J.; Windus, T. L.; Dupuis, M.; Montgomery, J. A.; see e.g.: Schmidt, M. W.; Baldridge, K. K.; Boatz, J. A.; Elbert, S. T.; Gordon, M. S.; Jensen, J. H.; Koseki, S.; Matsunaga, N.; Nguyen, K. A.; Su, S. J.; Windus, T. L.; Dupuis, M.; Montgomery, J. A. *J. Comput. Chem.* **1993**, *14*, 1347.

(14) Wachters, A. J. H. *J. Chem. Phys.* **1970**, *52*, 1033.

(15) Dunning, T. H.; Hay, P. J. *Methods of Electronic Structure Theory*; Plenum Press: New York, 1977.

(16) Huzinaga, S. *J. Chem. Phys.* **1965**, *42*, 1293.

(17) (a) The methodology was communicated to S. Shaik by M. W. Schmidt from Iowa State University. To obtain the five degenerate configurations, an initial GVB calculation is performed for the ^{5}D term of neutral Fe, using a Hückel guess with orbital reordering (IORDER(10) = 15, 10, 11, 12, 13, 14). Standard values for the fractional occupations and coupling coefficients are employed as recommended in the GAMESS[13] manual. The resulting GVB wave functions for Fe are then subject to a state averaged MCSCF calculation, leading to five averaged states of the type $4s^23d^6$. These averaged states are subsequently used for Fe^+ as an initial guess in an averaged MCSCF calculation of the ^{6}D term. The use of C_1 symmetry in \$DRT (\$DRT GROUP=C1 FORS=.T. NMCC=9 NDOC=1 NALP=5 \$END) ensures that all five spatial configuration state functions (CSF's) are kept in the CI function and their density averaged in order to obtain five spatially degenerate components of the ^{6}D multiplet. The spin−orbit coupling CI code subsequently uses all the possible sextet spin functions of the five spatial wave functions (use GROUP=C1), resulting in a 30 × 30 matrix for the SOC-CI Hamiltonian. (b) This is done by increasing the convergence criterion for the Davidson eigenvector routine (CVGTOL=1.0E-10) in the GUGDIA group in the GAMESS-USA 95 program.[13]

(18) Moore, C. E. *Atomic Energy Levels*; NSRDS-NBS: US GPO 35, DC, 1971.

(19) See pps 214−215 of ref 8a above.

Scheme 1

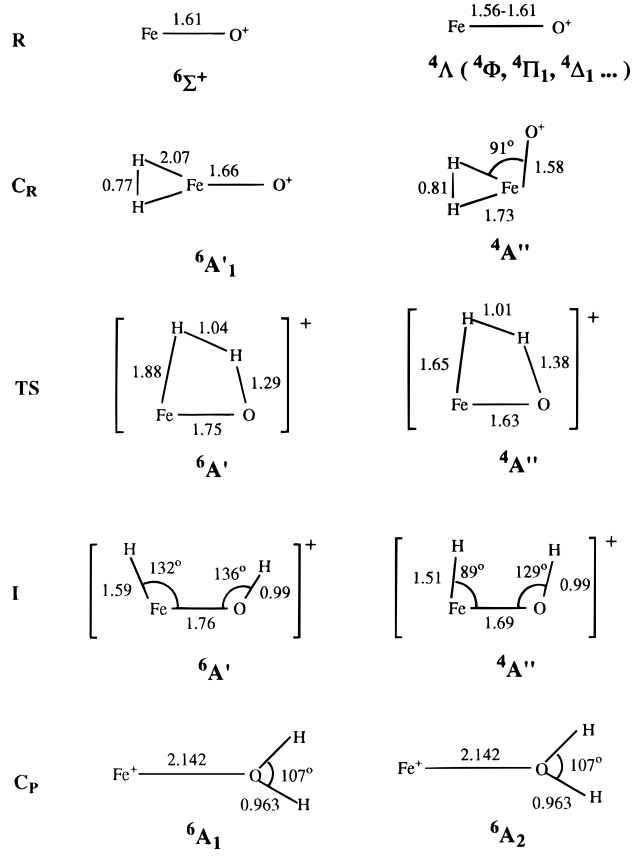

determinants. Here we expanded the angular momentum determinants, based on complex orbitals, into linear combinations of symmetry-adapted determinants based on real orbitals.

A typical SOC calculation for the target species involves between 8 000 and 30 000 CSF's and takes on the average, depending on the point group symmetry, 10−100 CPU hours on an IBM RS-6000/590 Workstation with 256MB RAM.

Results

The SOC calculations for the process in eq 1 were performed using the Berlin group's[2e,21] optimized geometries (Scheme 1) for the critical species which occur along the reaction path in Figure 1. Since we are interested in the pairwise SOC interactions which lend probabilities to crossovers between sextet and quartet states, we calculated for each molecular species the following SOC matrix element:

$$\langle \mathbf{H}_{SO} \rangle = \langle {}^6\Psi_1 | \mathbf{H}_{SO} | {}^4\Psi_2 \rangle \qquad (3)$$

A. FeO^+. The MO scheme for the $^6\Sigma^+$ state is shown in the left side of Figure 2 using the leading configuration of the MCSCF wave function. The orbital block in the frame is quasidegenerate[2e] and involves the δ orbitals which are pure d-AO's on Fe, the 2π orbitals which are antibonding FeO^+ MO's made from Fe(d_π)−O(p_π) combinations, and finally, the 3σ orbital which is largely a hybrid on Fe of the type d_{z^2}–s−p. Orbital excitations within the quasidegenerate manifold lead to a few low-lying quartet states having angular momenta $\Lambda = 0$, 1, 2, 3, and 4 (labeled as Σ, Π, Δ, Φ, and Γ). The energy ordering of these states based on results by Berlin's group[2e,22] is shown on the right-hand side of Figure 2, where in parentheses

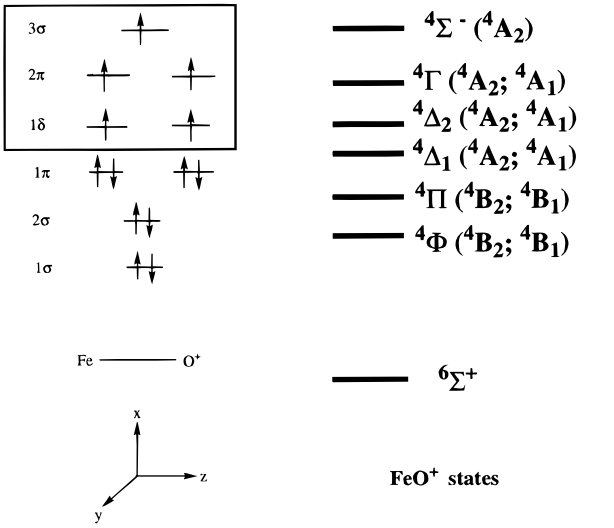

Figure 2. Molecular orbital (MO) scheme for the $^6\Sigma^+$ state of FeO^+ (left-hand side) and the corresponding state ordering (right-hand side).

Table 1. SOC Matrix Elements (in cm^{-1}) between $^6\Sigma^+$ and Some Quarted States, $^4\Lambda$, of FeO^+ [a]

quartet state	orbital occupancy[b]	$\langle H_{SO}\rangle_r$	$\langle S_1 = {}^5/_2; Ms_1 \vert S_2 = {}^3/_2; Ms_2\rangle$[c,d]
$^4\Phi$	$1\delta^3 2\pi^1 3\sigma^1$	$r = x, y, z$	0
$^4\Pi$	$1\delta^3 2\pi^1 3\sigma^1$	$r = x, y$[e]	$\langle {}^5/_2 \vert {}^3/_2\rangle = -178$
			$\langle {}^1/_2 \vert {}^3/_2\rangle = 56$
			$\langle {}^3/_2 \vert {}^1/_2\rangle = -138$
			$\langle -{}^1/_2 \vert {}^1/_2\rangle = 98$
			$\langle {}^1/_2 \vert -{}^1/_2\rangle = -98$
			$\langle -{}^3/_2 \vert -{}^1/_2\rangle = 138$
			$\langle -{}^1/_2 \vert -{}^3/_2\rangle = -56$
			$\langle -{}^5/_2 \vert -{}^3/_2\rangle = 178$
$^4\Delta_1$	$1\delta^3 2\pi^3$	$r = x, y, z$	0
$^4\Delta_2$	$1\delta^2 2\pi^2 3\sigma^1$	$r = x, y, z$	0
$^4\Gamma$	$1\delta^2 2\pi^2 3\sigma^1$	$r = x, y, z$	0
$^4\Sigma^-$	$1\delta^2 2\pi^2 3\sigma^1$	$r = z$	$\langle {}^3/_2 \vert {}^3/_2\rangle = -179$
			$\langle {}^1/_2 \vert {}^1/_2\rangle = -220$
			$\langle -{}^1/_2 \vert -{}^1/_2\rangle = -220$
			$\langle -{}^3/_2 \vert -{}^3/_2\rangle = -179$

[a] The bond length for FeO^+ is given in Scheme 1. The axes assignments are given in Figure 2. Accuracy here and elsewhere is ±1 cm^{-1}. [b] These are angular momentum (complex) orbitals. [c] All matrix elements were verified also at the C_s point group symmetry between $^6A'$ and $^4A''$, $^4A'$ states. [d] The atomic constant ζ_{Fe^+} of Fe^+ is calculated to be 407.3 cm^{-1}. [e] Only the *x* component is shown. The *y* component has the same absolute value with opposite sign.

we indicate the C_{2v} symmetry species contributed by each angular momentum state.[10a,d,e] It is apparent that when the angular momentum quantum number is different from zero, the corresponding state gives rise to two C_{2v} symmetry species. Thus, for example, by calculating the various MCSCF roots for $^4B_2$ and $^4B_1$ state symmetries, it is possible to pair up the two particular components which make up the $^4\Pi$ state, as well as those two components which make up the $^4\Phi$ state, and so on. Calculating, then, all the possible SOC matrix elements, types $\langle {}^6A_1 | \mathbf{H}_{SO} | {}^4B_{1,2}\rangle$, and rechecking them by performing the calculations at the C_s point group, enabled us to verify the SOC assignments which are collected in Table 1. The effect of the substate splitting of the higher angular momentum states on the SOC matrix elements with $^6\Sigma^+$ was not considered.

Recalling that the internuclear Fe- - -O axis is the *z* axis (in the appropriate point group) we note four trends in Table 1: (i) The only states which yield nonvanishing SOC with $^6\Sigma^+$ are $^4\Pi$ and $^4\Sigma^-$. (ii) The $^6\Sigma^+/^4\Pi$ coupling leads to *x* and *y* components (perpendicular to the molecular axis) of the SOC matrix element, while the $^6\Sigma^+/^4\Sigma^-$ coupling leads to a *z*

(20) Hiberty, P. C.; Leforestier, C. *J. Am. Chem. Soc.* **1978**, *100*, 2109.
(21) Fiedler, A.; Hrusak, J.; Schwarz, H. *Z. Phys. Chem.* **1992**, *175*, S15.
(22) Fiedler, A.; Hrusak, J.; Koch, W.; Schwarz, H. *Chem. Phys. Lett.* **1993**, *211*, 242.

component along the molecular axis. (iii) The *x*, *y* components couple spin-sublevels (substates), which differ by ±1 units from the Ms quantum number, while the *z* component couples substates with ΔMs = 0. (iv) The SOC matrix elements are significantly smaller than the atomic constant of Fe^+.

B. $FeO^+\cdots H_2$; ^{4,6}CR and ^{4,6}TS. The interaction of FeO^+ with H_2, to form the clusters C_R of Figure 1, lifts the degeneracies in the 1δ and 2π orbital subsets in Figure 2, and leads also to intermixing among the 3σ, 1δ, and 2π orbitals. As long as the intermolecular distances are sufficiently large, the quasidegeneracy of this orbital block is retained and the ground state is the sextet (Figure 1). As the $FeO^+\cdots H_2$ distance decreases and stronger orbital mixings ensue, the quartet state becomes the ground state.[2e] Clearly, somewhere in between the clusters C_R and the TS's, the two spin states cross one another. Finding the seam of the crossing points of the two states at the CASPT2 level,[23] which is the level used at the original study,[2e] is too complicated, and may even be irrelevant since under gas-phase conditions the system will not necessarily invert the spin at the lowest energy crossing point. Thus, we calculated the SOC patterns at the four geometric structures, corresponding to the two C_R's and the two TS's (Scheme 1), with the expectation that these limits will provide us a reasonable clue on the variation or lack thereof of the SOC matrix element in the region of the crossing. These corresponding sextet−quartet SOC matrix elements are collected in Table 2.

Entries 1−4 show the SOC matrix elements between the $^6A_1$ ground state of the ^6C_R cluster (Figure 1) and the four lowest lying quartet states, $^4B_1$, $^4B_2$, $^4A_2$, and $^4A_1$. A few trends are apparent and were verified by repeating the SOC calculations at the C_s point group symmetry: (i) The $^6A_1$ state couples with $^4B_2$, $^4B_1$, and $^4A_2$, giving rise respectively to in-plane *x*,*y* components and a perpendicular *z* component of the SOC matrix element. The coupling with the $^4A_1$ state is zero. (ii) By analogy to the trends in Table 1, here too the *x* and *y* components couple substates which differ by ΔMs = ±1 in their magnetic quantum numbers, while the *z* component couples substates with ΔMs = 0. (iii) Comparison of Table 2 to Table 1 (and later to Table 3) shows that irrespective of the magnitude of the individual SOC matrix elements, their ratios are constants typical of the *x*,*y* or *z* components. For the *x*,*y* components there are four unique SOC elements with ratios of 1:0.31623:0.7750:0.5477, in respective order, while for the *z* component the ratios for the unique elements are 1:1.2247.

At the geometry of the ^4C_R cluster, the ground state is $^4A''$ and the first sextet state is $^6A'$. Now, the *z* axis is perpendicular to the molecular *x*,*y* plane. The calculated SOC matrix element was restricted now to the two lowest spin states and is given in entry 5 in Table 2. Entry 6 shows the $^6A'/^4A''$ coupling at the geometry of the ^{6}TS, while entry 7 gives the same coupling type for the geometry of the ^{4}TS species, the latter being the lowest TS for the bond insertion step (Figure 1). In entries 5−7, the coupling involves in-plane *x*,*y* components and couples substates with ΔMs = ±1.

By comparing the SOC matrix elements in Tables 1 and 2, it is apparent that they undergo a gradual reduction, in the order SOC[R(FeO^+)] > SOC[C_R(FeO^+/H_2)] > SOC[TS($FeOH_2^+$)].

C. The Exit Channel: $Fe^+\cdots OH_2$ ($^{4,6}C_P$) and Fe^+ (^{6}D, ^{4}F, and ^{4}D). The ground state of the product cluster C_P $Fe^+\cdots OH_2$ is either $^6A_2$ or $^6A_1$.[21,24] In accord with previous results,[21] the two states were found to be extremely close (0.3 kcal/mol).

Table 2. SOC Matrix Elements (in cm^{-1}) in the FeO^+/H_2 Clusters (C_R) and Transition States (TS) for the Bond Insertion Step[a]

entry	state 1	state 2[b]	$\langle \mathbf{H}_{SO}\rangle_r$	$\langle S_1 = {}^5/_2; Ms_1 \vert S_2 = {}^3/_2; Ms_2\rangle$
1	^6C_R; $^6A_1$	$^4B_2$	$r = x$	$\langle {}^5/_2 \vert {}^3/_2\rangle = 121$ $\langle {}^1/_2 \vert {}^3/_2\rangle = -38$ $\langle {}^3/_2 \vert {}^1/_2\rangle = 94$ $\langle -{}^1/_2 \vert {}^1/_2\rangle = -66$ $\langle {}^1/_2 \vert -{}^1/_2\rangle = 66$ $\langle -{}^3/_2 \vert -{}^1/_2\rangle = -94$ $\langle -{}^1/_2 \vert -{}^3/_2\rangle = 38$ $\langle -{}^5/_2 \vert -{}^3/_2\rangle = -121$
2	^6C_R; $^6A_1$	$^4A_2$	$r = z$	$\langle {}^3/_2 \vert {}^3/_2\rangle = 64$ $\langle {}^1/_2 \vert {}^1/_2\rangle = 79$ $\langle -{}^1/_2 \vert -{}^1/_2\rangle = 79$ $\langle -{}^3/_2 \vert -{}^3/_2\rangle = 64$
3	^6C_R; $^6A_1$	$^4B_1$	$r = y$	*c*
4	^6C_R; $^6A_1$	$^4A_1$	$r = x, y, z$	0
5	^4C_R; $^4A''$	$^6A'$	$r = x, y$	$\langle {}^5/_2 \vert {}^3/_2\rangle = -87; 49$ $\langle {}^1/_2 \vert {}^3/_2\rangle = 27; -16$ $\langle {}^3/_2 \vert {}^1/_2\rangle = -67; 38$ $\langle -{}^1/_2 \vert {}^1/_2\rangle = 47; -27$ $\langle {}^1/_2 \vert -{}^1/_2\rangle = -47; 27$ $\langle -{}^3/_2 \vert -{}^1/_2\rangle = 67; -38$ $\langle -{}^1/_2 \vert -{}^3/_2\rangle = -27; 16$ $\langle -{}^5/_2 \vert -{}^3/_2\rangle = 87; 49$
6	^{6}TS; $^6A'$	$^4A''$	$r = x, y$	$\langle {}^5/_2 \vert {}^3/_2\rangle = -46; 65$ $\langle {}^1/_2 \vert {}^3/_2\rangle = 15; -21$ $\langle {}^3/_2 \vert {}^1/_2\rangle = -36; 51$ $\langle -{}^1/_2 \vert {}^1/_2\rangle = 25; -36$ $\langle {}^1/_2 \vert -{}^1/_2\rangle = -25; 36$ $\langle -{}^3/_2 \vert -{}^1/_2\rangle = 36; -51$ $\langle -{}^1/_2 \vert -{}^3/_2\rangle = -15; 21$ $\langle -{}^5/_2 \vert -{}^3/_2\rangle = 46; -65$
7	^{4}TS; $^4A''$	$^6A'$	$r = x, y$	$\langle {}^5/_2 \vert {}^3/_2\rangle = 44; -84$ $\langle {}^1/_2 \vert {}^3/_2\rangle = -14; 26$ $\langle {}^3/_2 \vert {}^1/_2\rangle = 34; -65$ $\langle -{}^1/_2 \vert {}^1/_2\rangle = -24; 46$ $\langle {}^1/_2 \vert -{}^1/_2\rangle = 24; -46$ $\langle -{}^3/_2 \vert -{}^1/_2\rangle = -34; 65$ $\langle -{}^1/_2 \vert -{}^3/_2\rangle = 14; -26$ $\langle -{}^5/_2 \vert -{}^3/_2\rangle = -44; 84$

[a] The SOC matrix element (eq 3) is determined at the geometry corresponding to the species specified as "state 1". The geometries are given in Scheme 1. [b] Entries 1−3 were verified also in the C_s point group symmetry. [c] Entry 3 has the same absolute values of SOC matrix elements as in entry 1 but with opposite signs.

Two higher sextet states of $^6B_1$ and $^6B_2$ symmetry lie 3−5 kcal/mol above the ground states, while a second $^6A_1$ state lies still 9.2 kcal/mol above the ground states. The d-type orbitals of the complex resemble those in Fe^+, albeit with a small admixture of the oxygen's orbitals. As such, the five spatial sextet states can be traced to the degenerate $4s^13d^6$ configurations in the free Fe^+. Indeed by analogy to the ^{6}D state of Fe^+, here in $Fe^+\cdots OH_2$ too, there is SOC *within the sextet manifold*. This results in a mixing of the two degenerate ground state configurations $^6A_1$ and $^6A_2$, so that for all purposes the ground sextet state has a mixed $^6A_{1,2}$ character. Thus, in Table 3 the sextet state (see the column state 2) is represented by the mixed $^6A_{1,2}$ situation.

Above the sextet manifold we find 12 quartet states of $^4A_2$, $^4A_1$ $^4B_2$, and $^4B_1$ spatial symmetries. These states are nascent from the ^{4}F ($3d^7$) and ^{4}D ($4s^13d^6$) atomic states of Fe^+. The lowest states, of $^4A_2$, $^4A_1$ symmetries, were traced to the ^{4}D atomic situation ($4s^13d^6$) of Fe^+. These states as well as the lowest $^4B_2$ and $^4B_1$ states are indicated therefore in Table 3 as "^{4}D" (see the column state 1) to emphasize their atomic ancestry. Still higher in energy we find seven quartet states which could be traced to the ^{4}F atomic state of Fe^+ ($3d^7$), and as such are indicated in Table 3 as "^{4}F" states. As mentioned already, our calculations underestimate the stability of the ^{4}F state, and this

(23) Andersson, K.; Malmqvist, P.-Å.; Roos, B. O. *J. Phys. Chem.* **1992**, *96*, 1218. Andersson, K.; Malmqvist, P.-Å.; Roos, B. O.; Sadlej, A. J.; Wolinski, K. *J. Phys. Chem.* **1992**, *94*, 5483.

(24) Rosi, M.; Bauschlicher, C. W., Jr. *J. Chem. Phys.* **1989**, *90*, 7264; **1990**, *92*, 1876.

Table 3. Selected SOC Matrix Elements (in cm^{-1}) in the Fe^+/OH_2 Cluster (^6C_p) at the Elimination Step[a,b]

entry	state 1	state 2	$\langle \mathbf{H}_{SO}\rangle_r$	$\langle S_1 = {}^5/_2; Ms_{1k}\|S_2 = {}^3/_2; Ms_{2k'}\rangle$[c–e]
1	$^6A_1$; $^6A_2$	"^{4}D"; $^4A_2$	$r = z$	$\langle {}^3/_2\|{}^3/_2\rangle = 79; 0$ $\langle {}^1/_2\|{}^1/_2\rangle = 96; 0$
2	$^6A_1$; $^6A_2$	"^{4}D"; $^4A_1$	$r = z$	*f*
3	$^6A_1$; $^6A_2$	"^{4}D"; $^4B_2$	$r = x; y$	$\langle {}^5/_2\|{}^3/_2\rangle = -49; -39$ $\langle {}^1/_2\|{}^3/_2\rangle = 15; 12$ $\langle {}^3/_2\|{}^1/_2\rangle = -38; -30$ $\langle -{}^1/_2\|{}^1/_2\rangle = 27; 21$
4	$^6A_1$; $^6A_2$	"^{4}D"; $^4B_1$	$r = y; x$	$\langle {}^5/_2\|{}^3/_2\rangle = -32; 39$ $\langle {}^1/_2\|{}^3/_2\rangle = 10; -12$ $\langle {}^3/_2\|{}^1/_2\rangle = -25; 30$ $\langle -{}^1/_2\|{}^1/_2\rangle = 18; -21$
5	$^6A_1$; $^6A_2$	"^{4}F"; $^4A_2$	$r = z$	$\langle {}^3/_2\|{}^3/_2\rangle = -5; (0)$ $\langle {}^1/_2\|{}^1/_2\rangle = -6; (0)$
6	$^6A_1$; $^6A_2$	"^{4}F"; $^4A_1$	$r = z$	*g*
7	$^6A_1$; $^6A_2$	"^{4}F"; $^4B_2$	$r = x; y$	$\langle {}^5/_2\|{}^3/_2\rangle = -8; 53$ $\langle {}^1/_2\|{}^3/_2\rangle = 3; -17$ $\langle {}^3/_2\|{}^1/_2\rangle = -6; 41$ $\langle -{}^1/_2\|{}^1/_2\rangle = 4; -29$
8	$^6A_1$; $^6A_2$	"^{4}F"; $^4B_1$	$r = y; x$	$\langle {}^5/_2\|{}^3/_2\rangle = -45; -27$ $\langle {}^1/_2\|{}^3/_2\rangle = 14; 9$ $\langle {}^3/_2\|{}^1/_2\rangle = -35; -21$ $\langle -{}^1/_2\|{}^1/_2\rangle = 25; 15$
9	$^6A_1$; $^6A_2$	"^{4}F"; 2^4A_2	$r = z$	$\langle {}^3/_2\|{}^3/_2\rangle = -2; 0$ $\langle {}^1/_2\|{}^1/_2\rangle = -3; 0$
10	$^6A_1$; $^6A_2$	"^{4}F"; 2^4B_2	$r = x; y$	$\langle {}^5/_2\|{}^3/_2\rangle = 69; 26$ $\langle {}^1/_2\|{}^3/_2\rangle = -22; -8$ $\langle {}^3/_2\|{}^1/_2\rangle = 53; 20$ $\langle -{}^1/_2\|{}^1/_2\rangle = -38; -14$
11	$^6A_1$; $^6A_2$	"^{4}F"; 2^4B_1	$r = y; x$	$\langle {}^5/_2\|{}^3/_2\rangle = 40; -64$ $\langle {}^1/_2\|{}^3/_2\rangle = -13; 20$ $\langle {}^3/_2\|{}^1/_2\rangle = 31; -49$ $\langle -{}^1/_2\|{}^1/_2\rangle = -22; 35$

[a] The geometry of ^6C_p is given in Scheme 1. [b] "^{4}D" means that the electronic structure of the Fe^+ moiety within the complex resembles the ^{4}D atomic situation ($4s^13d^6$), while "^{4}F" means the same with respect to the ^{4}F atomic situation ($3d^7$). [c] In each entry line, the matrix elements are $\langle {}^6A_1|\mathbf{H}_{SO}|{}^4\Psi_i\rangle$ and $\langle {}^6A_2|\mathbf{H}_{SO}|{}^4\Psi_i\rangle$, respectively. [d] Only unique matrix elements are shown. The rest can be completed following Tables 1 and 2. [e] The matrix elements $\langle {}^6B_{1,2}|\mathbf{H}_{SO}|{}^4\Psi_i\rangle$ are available from the authors. [f] The SOC matrix elements have the same values as in entry 1, but the ordering of the values in each line is switched, in accord with the selection rules. [g] The SOC matrix elements have the same values as in entry 5, but the signs are opposite, and the ordering of the values in each line is switched, in accord with the selection rules.

deficiency carries over to the $Fe^+\cdots OH_2$ complex. The more elaborate calculations by Rossi et al.[24] show that the lowest quartet states of $Fe^+\cdots OH_2$ are $^4A_2$ and $^4A_1$ which are nascent from the ^{4}F atomic situation, albeit with some mixing from ^{4}D and other atomic states. This blend of the atomic situations in the $Fe^+\cdots OH_2$ complex reflects the hybridization of the 4s and d_{z^2} orbitals (and to some extent $4p_z$ and $d_{x^2-y^2}$) in the presence of the H_2O ligand in the complex. The states within the quartet manifold mix among themselves via the SOC operator in complete analogy to the atomic situations ^{4}D and ^{4}F.

The SOC interactions within the same spin manifolds do not mix any quartet and sextet states. The requisite sextet−quartet SOC interactions for $Fe^+\cdots OH_2$ are collected in Table 3. To save space, we show only the SOC interactions of the sextet ground state(s) $^6A_{1,2}$ with quartet states from the "^{4}D" and "^{4}F" manifolds. The vanishing matrix elements are between states of identical spatial symmetry. All other situations lead to *x*,*y* or *z* components of SOC, by analogy to the preceding cases in Tables 1 and 2.

Focusing on the SOC interaction of $^6A_{1,2}$ with the $^4A_{1,2}$ quartet ground states of the "^{4}D" and "^{4}F" manifolds (entries 1,2 and 5,6 in Table 3), it is seen that the SOC matrix elements are either small (entries 1,2) or vanishingly small (entries 5,6). While the small size of these matrix elements may appear surprising, Table 4 shows that the same situation occurs for the sextet−quartet SOC in the free Fe^+. Thus, entries 1 and 2 in Table 3 are of the same order as those in entries 1,2 in Table 4 between ^{6}D ($4s^13d^6$) and the ^{4}D ($4s^13d^6$) atomic states, while entries 5 and 6 in Table 3 are similar to entries 5 and 6 in Table 4 for the ^{6}D ($4s^13d^6$)−^{4}F ($3d^7$) SOC. We may therefore conclude that the SOC interactions between the sextet and quartet ground states ($^6A_{1,2}$ with $^4A_{1,2}$) for $Fe^+\cdots OH_2$ resemble the patterns found for the parent atomic states of Fe^+. Moreover, as we approach the free Fe^+, the sextet−quartet SOC interaction gradually decreases until it reaches nearly zero between the ground state, ^{6}D, and the first excited state, ^{4}F, of Fe^+.

Table 4. Selected SOC Matrix Elements (in cm^{-1}) between the ^{6}D and ^{4}D, ^{4}F States of Fe^+, at the Exit of the Elimination Step

entry	state 1	state 2	$\langle \mathbf{H}_{SO}\rangle_r$	$\langle S_1 = {}^5/_2; Ms_{1k}\|S_2 = {}^3/_2; Ms_{2k'}\rangle$[a,b]
1	$^6A_1$; $^6A_2$	^{4}D; $^4A_2$	$r = z$	$\langle {}^3/_2\|{}^3/_2\rangle = 53; 0$ $\langle {}^1/_2\|{}^1/_2\rangle = 64; 0$
2	$^6A_1$; $^6A_2$	^{4}D; $^4A_1$	$r = z$	*c*
3	$^6A_1$; $^6A_2$	^{4}D; $^4B_2$	$r = x; y$	$\langle {}^5/_2\|{}^3/_2\rangle = -31; 46$ $\langle {}^1/_2\|{}^3/_2\rangle = 10; -14$ $\langle {}^3/_2\|{}^1/_2\rangle = -24; 35$ $\langle -{}^1/_2\|{}^1/_2\rangle = 17; -25$
4	$^6A_1$; $^6A_2$	^{4}D; $^4B_1$	$r = y; x$	$\langle {}^5/_2\|{}^3/_2\rangle = -90; 46$ $\langle {}^1/_2\|{}^3/_2\rangle = 28; -14$ $\langle {}^3/_2\|{}^1/_2\rangle = -69; 35$ $\langle -{}^1/_2\|{}^1/_2\rangle = 49; -25$
5	$^6A_1$; $^6A_2$	^{4}F; $^4A_2$	$r = z$	$\langle {}^3/_2\|{}^3/_2\rangle = -5; 0$ $\langle {}^1/_2\|{}^1/_2\rangle = -5; 0$
6	$^6A_1$; $^6A_2$	^{4}F; $^4A_1$	$r = z$	$\langle {}^3/_2\|{}^3/_2\rangle = 0; 6$ $\langle {}^1/_2\|{}^1/_2\rangle = 0; 7$
7	$^6A_1$; $^6A_2$	^{4}F; $^4B_2$	$r = x; y$	$\langle {}^5/_2\|{}^3/_2\rangle = -8; 1$ $\langle {}^1/_2\|{}^3/_2\rangle = -6; \approx 0$ $\langle {}^3/_2\|{}^1/_2\rangle = 3; \approx -0$ $\langle -{}^1/_2\|{}^1/_2\rangle = -4; \approx 0$
8	$^6A_1$; $^6A_2$	^{4}F; $^4B_1$	$r = y; x$	$\langle {}^5/_2\|{}^3/_2\rangle = 1; -1$ $\langle {}^1/_2\|{}^3/_2\rangle = 1; -1$ $\langle {}^3/_2\|{}^1/_2\rangle = \approx -0; \approx 0$ $\langle -{}^1/_2\|{}^1/_2\rangle = \approx 0; -1$
9	$^6A_1$; $^6A_2$	^{4}F; 2^4A_2	$r = z$	*d*
10	$^6A_1$; $^6A_2$	^{4}F; 2^4B_2	$r = x; y$	$\langle {}^5/_2\|{}^3/_2\rangle = 3; -8$ $\langle {}^1/_2\|{}^3/_2\rangle = 3; -6$ $\langle {}^3/_2\|{}^1/_2\rangle = -1; 3$ $\langle -{}^1/_2\|{}^1/_2\rangle = 2; -5$
11	$^6A_1$; $^6A_2$	^{4}F; 2^4B_1	$r = y; x$	$\langle {}^5/_2\|{}^3/_2\rangle = -7; -8$ $\langle {}^1/_2\|{}^3/_2\rangle = -5; -6$ $\langle {}^3/_2\|{}^1/_2\rangle = 2; 3$ $\langle -{}^1/_2\|{}^1/_2\rangle = -4; -5$

[a] In each entry line, the matrix elements are $\langle {}^6A_1|\mathbf{H}_{SO}|{}^4\Psi_i\rangle$ and $\langle {}^6A_2|\mathbf{H}_{SO}|{}^4\Psi_i\rangle$, respectively. [b] Only unique matrix elements are shown. The rest can be completed following Tables 1 and 2. [c] The SOC matrix elements have the same values as in entry 1, but the ordering in each line is switched. [d] The SOC matrix elements have the same values as in entry 6, but the ordering in each line is switched.

Discussion

A. Patterns of SOC Matrix Elements. The above results show that the sextet−quartet SOC matrix elements are highly anisotropic, depending on symmetry as well as on the match-up situation of the substates of the two spin states, and with different selectivities for the in-plane *x*,*y* and perpendicular *z* components of the SOC. The ratios of the SOC elements for the different pairs of substates are constants, typical of the *x*,*y* and *z* components, and carry over irrespective of the identity

of the electronic states. In addition, the SOC matrix elements vary for different species along the reaction coordinate: starting high at the entrance channel, decreasing along the bond insertion process, and going to nearly zero at the Fe^+ exit channel between the ^{6}D ground state and the ^{4}F first excited state. Some of these patterns are not immediately obvious and require conceptualization. Even though rules for SOC are known in principle,[8,9a−d,j] it is not clear how they are precisely manifested in complex molecular situations of low symmetry, and more importantly *how they are derived from the electronic structure of the states*. This is especially true for transition metal reactivity where the spin states are more complex than the singlet−triplet situations in organic chemistry. Thus, some reiteration of SOC ideas would be necessary to create a coherent discussion of the matter.

In the general situation, we need to consider the SOC between two multiconfigurational wave functions $\Psi_1(S_1;\mathrm{Ms}_{1k})$ and $\Psi_2(S_2;\mathrm{Ms}_{2k'})$ which belong to different spin states, S_1 and S_2, and have spin-sublevles (substates) Ms_{1k} and $\mathrm{Ms}_{2k'}$, respectively. Each wave function is given therefore by the appropriate linear combination of spin-adapted configurations in eqs 4a and 4b, where the c_I and c_J are real number coefficients of the MCSCF configurations.

$$\Psi_1(S_1;\mathrm{Ms}_{1k}) = \sum_I c_I \Phi_I(S_1;\mathrm{Ms}_{1k}) \tag{4a}$$

$$\Psi_2(S_2;\mathrm{Ms}_{2k'}) = \sum_J c_J \Phi_J(S_2;\mathrm{Ms}_{2k'}) \tag{4b}$$

Following the one-electron approximation,[8a,b,11a,b] the SOC Hamiltonian is given by a sum of one-electron contributions, expressed in eq 5

$$\mathbf{H}_{\mathrm{SO}} = \sum_i \mathbf{h}_{\mathrm{SO}}(i); \qquad \mathbf{h}_{\mathrm{SO}}(i) = \sum_K A_{iK}\mathbf{L}_{iK}\cdot\mathbf{S}_i;$$
$$A_{iK} = \alpha^2/2(Z_K^*/R_{iK}^3) \tag{5}$$

where the A_{iK} term is an operator which acts only on the radial part of the wave function, and includes terms defined in eq 2. Since $\mathbf{h}_{\mathrm{SO}}(i)$ is a mono-electronic Hamiltonian, it will couple only those configurations $\Phi_I(S_1;\mathrm{Ms}_{1k})$ and $\Phi_J(S_2;\mathrm{Ms}_{2k'})$ in eq 4 that either have the same electron occupation or differ at most by *a single-electron shift from spin orbital* $\langle\mu|$ *to spin orbital* $|\nu\rangle$. Most of the situations pertaining to the present paper correspond to the second case. As such, the configuration matrix element will consist of SOC matrix elements between the spin molecular orbitals which differ in one-electron occupancy in the two configurations, i.e.,

$$\langle\mathbf{H}_{\mathrm{SO}}\rangle_{I,J;k,k'} = n_{kk'}N_{Ik}N_{Jk'}c_Ic_J\langle\varphi_\mu\theta_\mu|\mathbf{h}_{\mathrm{SO}}|\varphi_\nu\theta_\nu\rangle;$$
$$\theta = \alpha \text{ and/or } \beta \text{ spin} \tag{6}$$

where the φ is the space part of the molecular orbital, θ the spin of the electron which is shifted from φ_μ (in Φ_I) to φ_ν (in Φ_J), and the N's the configuration's normalization constants which depend on the identity of the substates k and k'. The $n_{kk'}$ factor is the number of identical orbital terms which are contributed from the coupling of a given pair of Ms configurations.

The part of the SOC matrix element that carries the symmetry and substate selectivity involves the $\mathbf{L}\cdot\mathbf{S}$ operator,[8,9a−d,j] where $\mathbf{L}$ is the angular orbital momentum operator, while $\mathbf{S}$ is the spin operator. The $\mathbf{L}\cdot\mathbf{S}$ operator can be written as a sum of Cartesian components, or in terms of ladder operators.[8a] Thus, the expectation value of the $\mathbf{L}\cdot\mathbf{S}$ operator will have x, y and z components in the Cartesian representation or alternately appropriate "components" in the ladder representation. These components are expressed in eqs 7a and 7b.

$$\langle\varphi_\mu\theta_\mu|\mathbf{L}\cdot\mathbf{S}|\varphi_\nu\theta_\nu\rangle = \langle\varphi_\mu|l_x|\varphi_\nu\rangle\langle\theta_\mu|\boldsymbol{S}_x|\theta_\nu\rangle + \langle\varphi_\mu|l_y|\varphi_\nu\rangle\langle\theta_\mu|\boldsymbol{S}_y|\theta_\nu\rangle + \langle\varphi_\mu|l_z|\varphi_\nu\rangle\langle\theta_\mu|\boldsymbol{S}_z|\theta_\nu\rangle \tag{7a}$$

$$\langle\varphi_\mu\theta_\mu|\mathbf{L}\cdot\mathbf{S}|\varphi_\nu\theta_\nu\rangle = \langle\varphi_\mu|l_z|\varphi_\nu\rangle\langle\theta_\mu|\boldsymbol{S}_z|\theta_\nu\rangle + 0.5[\langle\varphi_\mu|l_+|\varphi_\nu\rangle\langle\theta_\mu|\boldsymbol{S}_-|\theta_\nu\rangle + \langle\varphi_\mu|l_-|\varphi_\nu\rangle\langle\theta_\mu|\boldsymbol{S}_+|\theta_\nu\rangle] \tag{7b}$$

If we index the components by the general subscript r, we can write for the r component of the SOC matrix element the expression in eq 8 which is based on the combination of eqs 6 and 7, and assumes that the dominant SOC terms are monocentric.[11a] Equation 8 specifies the r component of the SOC matrix element that arises from coupling of substates k and k' belonging respectively to two configurations Φ_I and Φ_J, themselves constituents of the spin states $\Psi_1(S_1)$ and $\Psi_2(S_2)$.

$$[\langle\mathbf{H}_{\mathrm{SO}}\rangle_r]_{I,J;k,k'} = n_{kk'}N_{Ik}N_{Jk'}c_Ic_J\sum_K \xi_K\langle\varphi_\mu|l_{rK}|\varphi_\nu\rangle\langle\theta_\mu|\boldsymbol{S}_r|\theta_\nu\rangle;$$
$$\xi_K = \langle\varphi_\mu|A_{iK}|\varphi_\nu\rangle \qquad \text{for} \qquad r = x, y, z$$
$$(0.5\langle\varphi_\mu|A_{iK}|\varphi_\nu\rangle \text{ for a ladder term}) \tag{8}$$

The total r component will arise from the summation of all the configurations in the MCSCF wave functions (eqs 4a and 4b). The atomic constant terms, ξ_K, depend on the effective nuclear charge Z_K^* exerted on the valence electrons, and thereby gauges the strength of any SOC matrix element which is allowed by the angular momentum and spin terms in eq 8.

B. Selection Rules. The SOC selection rules derive from the conditions which produce simultaneously nonvanishing spin, $\langle\theta_\mu|\boldsymbol{S}_r|\theta_\nu\rangle$, and orbital, $\langle\varphi_\mu|l_{rK}|\varphi_\nu\rangle$, factors.

(1) The Spin Factors, $\langle\boldsymbol{\theta_\mu}|\boldsymbol{S}_r|\boldsymbol{\theta_\nu}\rangle$. The spin factors, which are discussed in many sources,[8a,b,9a−d] yield either a 0 or 0.5 expectation value of spin angular momentum (in units of $\hbar$, dropping signs and complex numbers). Since the spin functions are eigenfunctions of $\boldsymbol{S}_z$, the only non-zero z component is when θ_μ and θ_ν are identical, i.e., only when the coupled substates involve the same number of α and β spin orbitals and hence the same Ms quantum number. Since $\boldsymbol{S}_x$ and $\boldsymbol{S}_y$ convert α spin to β spin and vice versa, the nonvanishing spin components will involve nonidentical spin functions $\theta_\mu \neq \theta_\nu$, i.e., when the coupled substates differ in their number of α and β spin orbitals such that $\mathrm{Ms}_{1k} = \mathrm{Ms}_{2k'} \pm 1$. The z and x,y selection rules are specified in eq 9.

If

$$\mathrm{Ms}_{1k} = \mathrm{Ms}_{2k'}(\Delta\mathrm{Ms}_{1k,2k'} = 0); \qquad \Rightarrow \langle\mathbf{H}_{\mathrm{SO}}\rangle_z \neq 0 \tag{9a}$$

If

$$\mathrm{Ms}_{1k} = \mathrm{Ms}_{2k'} \pm 1(\Delta\mathrm{Ms}_{1k,2k'}) = \pm 1;$$
$$\Rightarrow \langle\mathbf{H}_{\mathrm{SO}}\rangle_{x,y}; \langle\mathbf{H}_{\mathrm{SO}}\rangle_{\pm} \neq 0 \tag{9b}$$

Since the $\boldsymbol{S}_\pm$ operators are simply linear combinations of the $\boldsymbol{S}_{x,y}$ operators, the selection rules are identical in the two representations.

(2) The Orbital Factors, $\langle\boldsymbol{\varphi_\mu}|l_{rK}|\boldsymbol{\varphi_\nu}\rangle$. For linear molecules, the orbitals are eigenfunctions of the orbital momentum operator and it is easier to use the ladder representation, while for nonlinear molecules the Cartesian representation must be used. In any representation, the angular momentum expectation values, $\langle\varphi_\mu|l_{rK}|\varphi_\nu\rangle$, are either zero or given by $m_{\mu\nu}$, which is a number depending on the orbitals φ_μ and φ_ν, to be discussed later in Table 5.

(a) The Ladder Representation. When the orbitals are eigenfunctions of l_z, then the orbital factor will be non-zero only if the momentum quantum number, λ, is non-zero and identical for the two orbitals. The condition will be met only when the configurations, Φ_I and Φ_J, as well as their corresponding states Ψ_1 and Ψ_2, all have the same total angular momentum quantum number Λ, as given by eq 10a.

The operator l_+ acts on an orbital by raising its angular momentum by a unity, while the corresponding l_- operator's action is precisely the opposite. This means that SOC will be maintained only if the orbitals and the states differ by a unit of angular momentum, as expressed in eq 10b.

If

$$\Lambda_1 = \Lambda_2(\lambda_\mu = \lambda_\nu \neq 0 \text{ and } \Delta\Lambda = 0); \qquad \Rightarrow \langle \mathbf{H}_{SO} \rangle_z \neq 0 \tag{10a}$$

If

$$\Lambda_1 = \Lambda_2 \pm 1; \qquad \lambda_\mu = \lambda_\nu \pm 1; \qquad \Rightarrow \langle \mathbf{H}_{SO} \rangle_\pm \neq 0 \tag{10b}$$

(b) The Cartesian Representation. Applying the Cartesian representation to eq 7a allows us to derive symmetry as well as orientation rules for the orbitals which are involved in the SOC matrix element. Table 5 details the transformation properties of the d-AO's under the operation of the $l_{x,y,z}$ operators. There is an analogy to the transformation properties of the p-AO's.[8b,9a−d] The $l_{x,y,z}$ operators act on a Cartesian p-AO in two ways: first the operator eliminates any p-AO on the same axis as the operator itself, e.g., $l_z|p_z\rangle = 0$, and second, the operator rotates the p-AO about the Cartesian axis of the operator, e.g., l_x rotates functions about the x axis. Consequently, the nonvanishing angular momentum terms involve cyclic permutations of the x,y,z axes over the two p-AO's and the operator, e.g., $\langle p_x|l_z|p_y\rangle \neq 0$. Thus, a non-zero angular momentum expectation value is produced along the normal to the plane defined by a pair of p-AO's when they are perpendicularly oriented.

The situation with d-AO's is given in Table 5. *As a general rule, the d-orbital pairs which create non-zero angular momentum along a given axis involve d-AO's mutually related by a rotation about this axis*. For example, l_x rotates the d_{xy} AO around the x axis to a d_{xz} AO, and as such, the integral $\langle d_{xz}|l_x|d_{xy}\rangle$ has non-zero angular momentum about the x axis. In contrast, $\langle d_{x^2-y^2}|l_x|d_{xy}\rangle$ gives a zero angular momentum, because the two AO's are not mutually related by rotation about the x axis.

Symmetry can further assist to classify the angular momentum expectation values, $\langle \varphi_\mu|l_r|\varphi_\nu\rangle$ in the Cartesian representation. Thus, since the l_r operators transform as the real rotations R_r ($r = x,y,z$) of the point group,[8a,b,9c,j] the expectation values will vanish unless the direct product of the irreducible representations, Γ, of orbitals is identical to the representation of the corresponding real rotation R_r ($r = x,y,z$) of the point group. The symmetry selection rules follow in eqs 11a and 11b, in hierarchy, from the orbital to the state level:

If

$$\Gamma(\varphi_\mu)\otimes\Gamma(\varphi_\nu) = \Gamma(\Phi_I)\otimes\Gamma(\Phi_J) = \Gamma(\Psi_1)\otimes\Gamma(\Psi_2) = \Gamma(R_z); \qquad \Rightarrow \langle \mathbf{H}_{SO} \rangle_z \neq 0 \tag{11a}$$

If

$$\Gamma(\varphi_\mu)\otimes\Gamma(\varphi_\nu) = \Gamma(\Phi_I)\otimes\Gamma(\Phi_J) = \Gamma(\Psi_1)\otimes\Gamma(\Psi_2) = \Gamma(R_{x,y}); \qquad \Rightarrow \langle \mathbf{H}_{SO} \rangle_{x,y} \neq 0 \tag{11b}$$

Table 5. Transformation of d Orbitals Under the Operations of l_r ($r = x,y,z$) Operators[a]

l_r	d_{z^2}	$d_{x^2-y^2}$	d_{xy}	d_{xz}	d_{yz}
l_x	$-\sqrt{3}id_{yz}$	$-id_{yz}$	id_{xz}	$-id_{xy}$	$i(d_{x^2-y^2} - \sqrt{3}d_{z^2})$
l_y	$\sqrt{3}id_{xz}$	$-id_{xz}$	$-id_{yz}$	$i(d_{x^2-y^2} + \sqrt{3}d_{z^2})$	id_{xy}
l_z	0	$2id_{xy}$	$-2id_{x^2-y^2}$	id_{yz}	$-id_{xz}$

[a] The table entries are values of $l_i|d_i\rangle$ in $\hbar$ units.

The orbital level reveals that, only if the electron is allowed to shift *between two orbitals whose symmetry direct product matches that of one of the real rotations of the point group do we obtain a component of the SOC matrix element polarized along the axis of the rotation*. This result is a restatement of the orientation rules stated above (based on Table 5) for getting a non-zero orbital momentum expectation value from two d-orbitals.[25]

(c) The Effect of the Substate Identity. From a physical aspect, the different Ms values of a given S specify the allowed orientations of the spin vector relative to the principal axis, and these orientations determine eventually the strength of the coupling to the angular momentum vector $\mathbf{L}$ which has its own allowed orientations (specified by $\pm\Lambda$ in linear molecules) relative to the principal axis. As such, the SOC strength will depend on the identity of the Ms substates. In terms of electronic structure, the ratios between the SOC matrix elements of substate pairs (k, k') will be determined by the corresponding normalization constants, N_{Ik} and $N_{Jk'}$ and $n_{kk'}$; the latter factor enumerates the number of identical orbital SOC terms which are contributed by a given matrix element in eq 8.

The normalization constants are simple counts of the determinants that are required to form a spin-adapted configuration with a certain Ms value. For a given spin quantum number S, the Ms_k values are given as $Ms_k = 1/2(n_\alpha - n_\beta)$ where n_α and n_β are the numbers of α and β spins, respectively. The configuration with the highest Ms_k value has an all spin-up (α spins) electronic structure, and as such will be described by a single determinant wave function. The other configurations with lower Ms values will be described by an increasing number of determinants which correspond to the number of ways of arranging the electrons with α spins and β spins in the singly occupied orbitals. The number of determinants for a configuration having a given Ms_k and typified by the n_k number of singly occupied orbitals is $n_k!/(n_k - n_\alpha)!n_\alpha!$, and the normalization constant becomes therefore eq 12a.

$$N_{Ik} = 1/[n_k!/(n_k - n_\alpha)!n_\alpha!]^{1/2} \tag{12a}$$

$$[n_{kk'}]_{x,y} = [n_k!/(n_k - n_\alpha)!n_\alpha!]_{\min} \tag{12b}$$

$$[n_{kk'}]_z = 2[n_k!/(n_k - n_\alpha)!n_\alpha!]_{\min} \tag{12c}$$

$$[\langle \mathbf{H}_{SO} \rangle_r]_{I,J;k,k'}/[\langle \mathbf{H}_{SO} \rangle_r]_{I,J;l,l'} = n_{kk'}N_{Ik}N_{Jk'}/n_{ll'}N_{Il'}N_{Jl'} = W_{Ik,Jk'}/W_{Il,Jl'} \tag{12d}$$

Similarly, the factor $n_{kk'}$, in eq 8, depend on the number of determinant pairs which can contribute SOC terms, and is simply identical with the number of determinants (or twice that number) in that configuration described by the minimal number of spin arrangements; eq 12b for the x,y components and for eq 12c for the z component. The SOC matrix elements in eq 8 will be weighted by the product of N and n, and will thereby be

(25) This result brings to mind the classical analogy invoked by Salem and Rowland[9a] to explain the spin inversion which is promoted by SOC, that the "rotation" of the electron between the orbitals provides the torque which is required to invert the spin.[9a]

Table 6. Selection Rules for Non-Zero Spin−Orbit Coupling (SOC) between States with Different Spin Situations $\Psi_1(S_1,Ms_{1k})$ and $\Psi_2(S_2,Ms_{2k'})$

$\langle H_{SO}\rangle_r$	spin selection rule	angular momentum selection rule[a]	symmetry selection rule[b]
z	$\Delta Ms = 0$	$\Delta\Lambda = 0$; $\lambda_\mu = \lambda_\nu \neq 0$	$\Gamma(\Psi_1)\otimes\Gamma(\Psi_2) = \Gamma(R_z)$ $\Gamma(\varphi_\mu)\otimes\Gamma(\varphi_\nu) = \Gamma(R_z)$
x,y[c]	$\Delta Ms = \pm 1$	$\Delta\Lambda = \pm 1$; $(\lambda_\mu = \lambda_\nu \pm 1)$	$\Gamma(\Psi_1)\otimes\Gamma(\Psi_2) = \Gamma(R_x, R_y)$ $\Gamma(\varphi_\mu)\otimes\Gamma(\varphi_\nu) = \Gamma(R_x, R_y)$

[a] λ_μ, λ_ν refer to the orbital angular momenta of orbitals $\varphi_{\mu,\nu}$; Λ refers to the total angular momentum. [b] φ_μ and φ_ν are the orbitals which differ in one electron occupancy in the configurations belonging to Ψ_1 and Ψ_2, respectively. [c] The same rules apply to the ladder components (see e.g., eq 10b).

diminished. It is convenient then to group these terms as a weighing factor, $W_{Ik,Jk'}$, so that the ratio of two SOC matrix elements, for pairs of substates (kk' and ll'), can can be predicted as given by eq 12d.

It is apparent that the ratio in eq 12d is a constant which does not depend on the identity of the states but is determined solely by the number of equivalent ways that are available for the configurations to arrange the spins (number of determinants) in the singly occupied orbitals. *Thus, the distribution of the spin sublevels over the available arrangements limits the number of matched situations which follow the selection rules and down sizes thereby the SOC between the two configurations, in proportion to the available ways for spin distribution.*

C. Application of the Selection Rules to the Species in the Reaction (Eq 1). Table 6 summarizes all the selection rules derived above. These rules and the d orbital transformations in Table 5 will serve as a basis to rationalize the computational results in Tables 1−4.

(1) General Symmetry, Angular Momentum, and Spin Considerations. The species in Figure 1 and Scheme 1 belong to the $C_{\infty v}$, C_{2v}, and C_s point groups. Since the ground sextet state in these groups belongs to the totally symmetric representation (with the exception of C_P which is a linear combination of $^6A_1$ and $^6A_2$), it follows *that this state can be coupled to quartet states which possess the same symmetry as the real rotations for the respective point group*. Using character tables and Table 6, we can make predictions about the patterns of SOC in the various species, as depicted in Figure 3, which specifies the state pairs which are coupled via the z or x,y components of SOC.

At the bottom part of Figure 3, we show the patterns of the substate coupling based on the spin selection rules. The match-up of the substates is shown by lines that connect the spin sublevels; no energy ordering is meant by the vertical placement of the sublevels. Thus, in Figure 3a the z component that couples substates of the same Ms leaves the $Ms = {}^5/_2$ substates of the sextet state uncoupled, while in Figure 3b the x,y components are seen to couple all the substates which differ by ± 1 unit of Ms. These general predictions are in line with the computational results in Tables 1−3.

The ratios of the SOC matrix elements for each pair of substates are obtained by use of eq 12d and are indicated in Figure 3 above the lines connecting the substate. As an example, consider the coupling of $Ms_1 = {}^3/_2$ to $Ms_2 = {}^1/_2$ in Figure 3b. The sextet configuration with $Ms_1 = {}^3/_2$ has 5 possibilities to distribute four α spins among 5 singly occupied orbitals, and as such is described by 5 determinants. The quartet configuration with $Ms_2 = {}^1/_2$ has 3 possibilities to distribute the two α spins over three orbitals and has therefore 3 determinants. Each of the 3 determinants of the quartet state finds a match, which differs by a single electron shift, among

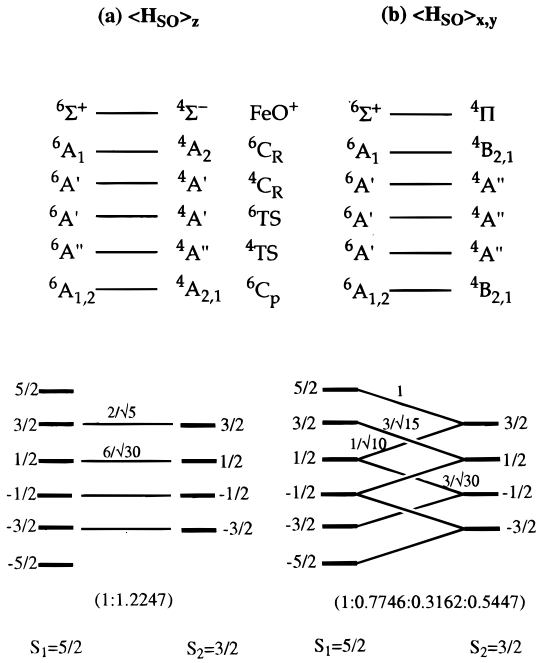

Figure 3. On top are state pairs that are coupled by SOC according to the symmetry rules, for the z component (a) and for the x,y components (b). At the bottom are schematic substate coupling diagrams. The weighing factors of the substate coupling (eq 12d) are shown above the corresponding coupling lines. The ratios of these weighing factors are displayed beneath each diagram (these ratios should be compared to the ratios of the SOC matix elements of different substates in Tables 1−4).

the 5 determinants of the sextet state. Therefore the SOC matrix element will be weighted by the factor $3/\sqrt{15}$. The ratios between the unique matrix elements are given underneath the substate-coupling diagrams in Figures 3a and 3b, and these ratios reproduce precisely the computed ratios of the SOC matrix elements in Tables 1−3.

(a) Orbital Effects on SOC in FeO$^+$. Having predicted the general trends of the computational data, we turn to analyze orbital related features of the specific systems. For FeO^+, in $C_{\infty v}$ symmetry, the states are angular momentum states and therefore the SOC selection rules must follow the angular momentum rules (see Table 6). It is seen from Figure 3 that the z component of the SOC couples the ground state $^6\Sigma^+$ with the $^4\Sigma^-$ state which possess the same total angular momentum, while the x,y components couple $^6\Sigma^+$ with the $^4\Pi$ states, which differ by one unit of angular momentum with respect to the sextet state. According to the angular momentum selection rules (Table 6) no other state can couple to $^6\Sigma^+$. These predictions[8a,b] are indeed followed by the computational results in Table 1.

To further understand the difference between the efficient $^6\Sigma^+/^4\Pi$ and $^6\Sigma^+/^4\Sigma^-$ couplings as opposed to the zero $^6\Sigma^+/^4\Phi$ coupling, we must inspect the orbital relationships which promote the SOC matrix elements. In the angular momentum representation, the fundamental $^6\Sigma^+$ ($^6A_1$ in C_{2v}) configuration is described by the orbital occupancy in Scheme 2 using the real representation of the orbitals along with their C_{2v} symmetry labels and Cartesian assignments. Expansion of the $^4\Pi$ and $^4\Phi$ fundamental configurations into the configurations based upon the real orbitals generates in each case four configurations which belong to two different symmetry species $^4B_1$ and $^4B_2$ and which are shown in Scheme 2. Since the two quartet states, $^4\Pi$ and $^4\Phi$, are made up from the same symmetry species, *symmetry analysis by itself is insufficient*, and we must therefore rely on the angular momentum realtionships in Table 5.

Scheme 2

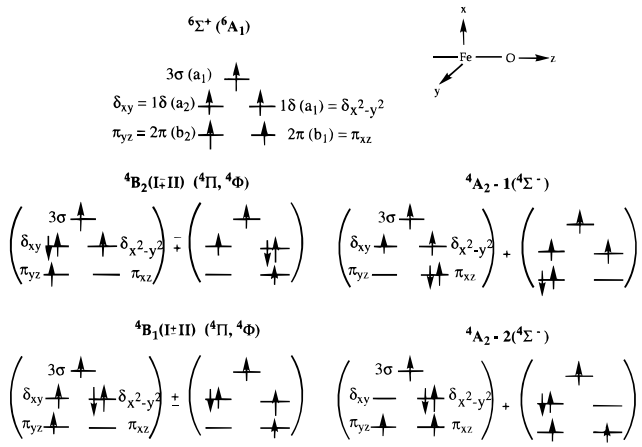

Consider the SOC between $^6\Sigma^+$ and the two $^4B_2$ components in Scheme 2. Each one of the $^4B_2$ determinants differs from the $^6\Sigma^+$ determinant by a single electron shift and as such is coupled with $^6\Sigma^+$ via the respective MO matrix element. After resolving the spin expectation values (0.5) and including all the constants from eq 8, the SOC matrix elements become eqs 13a and 13b.

$$\langle {}^6A_1({}^6\Sigma^+)|\mathbf{H}_{SO}|{}^4B_2(I)\rangle = 0.5(\zeta_{Fe} + \zeta_O)[\langle \pi_{xz}|l_x|\delta_{xy}\rangle - i\langle \pi_{xz}|l_y|\delta_{xy}\rangle] \quad (13a)$$

$$\langle {}^6A_1({}^6\Sigma^+)|\mathbf{H}_{SO}|{}^4B_2(II)\rangle = 0.5(\zeta_{Fe} + \zeta_O)[\langle \pi_{yz}|l_x|\delta_{x^2-y^2}\rangle - i\langle \pi_{yz}|l_y|\delta_{x^2-y^2}\rangle] \quad (13b)$$

The π_{xz} and π_{yz} orbitals are given as combinations of the iron's d AO's and the oxygen's p AO's, eq 14, and the 1δ orbitals are pure d AO's, d_{xz} and $d_{x^2-y^2}$.

$$2\pi_{xz} = c_{Fe}(d_{xz}) - c_O(p_x); \qquad 2\pi_{yz} = c_{Fe}(d_{yz}) - c_O(p_y) \quad (14)$$

Using the transformation of d AO's in Table 5, only the first term of both eqs 13a and 13b is non-zero, and given by:

$$\langle {}^6A_1({}^6\Sigma^+)|\mathbf{H}_{SO}|{}^4B_2(I)\rangle = 0.5c_{Fe}\zeta_{Fe}\langle d_{xz}|l_x|d_{xy}\rangle = 0.5c_{Fe}\zeta_{Fe} \quad (15a)$$

$$\langle {}^6A_1({}^6\Sigma^+)|\mathbf{H}_{SO}|{}^4B_2(II)\rangle = -0.5c_{Fe}\zeta_{Fe}\langle d_{yz}|l_x|d_{x^2-y^2}\rangle = -0.5c_{Fe}\zeta_{Fe} \quad (15b)$$

Summation of the above terms leads to zero SOC with the $^4\Phi$ state, while the difference of the terms for the $^4\Pi$ state gives a non-zero *x* component of the SOC matrix element, as summarized in eqs 16a and 16b, where the factor $2^{-1/2}$ is the normalization constant of the $^4B_2$ state.

$$\langle {}^6A_1({}^6\Sigma^+)|\mathbf{H}_{SO}|{}^4B_2({}^4\Phi)\rangle_x = 0 \quad (16a)$$

$$\langle {}^6A_1({}^6\Sigma^+)|\mathbf{H}_{SO}|{}^4B_2({}^4\Pi)\rangle_x = 2^{-1/2}c_{Fe}\zeta_{Fe} \quad (16b)$$

Turning back to Scheme 2, the $^4B_1$ components of $^4\Pi$ and $^4\Phi$ are linear combinations of $(\delta_{x^2-y^2})^2\delta_{xy}{}^1\pi_{yz}{}^13\sigma^1$ and $\delta_{xy}{}^2(\delta_{x^2-y^2})^1\pi_{xz}{}^13\sigma^1$. These $^4B_1$ components are generated from the $^6\Sigma^+$ state by electron shifts from π_{xz} to $\delta_{x^2-y^2}$ and from π_{yz} to δ_{xy}, which by analogy to the foregoing analysis (eqs 14−16) lead to the d-AO matrix elements, $\langle d_{xz}|l_y|d_{x^2-y^2}\rangle$ and $\langle d_{yz}|l_y|d_{xy}\rangle$. These d-AO relationships lead to *y* components of the angular momentum, which again add up for the $^4\Pi$ state and cancel out for the $^4\Phi$ state.

Consider now a fundamental $^4\Sigma^-$ configuration, the one which pairs up the π electrons in the angular momentum representation. The corresponding real representation is denoted in Scheme 2 as $^4A_2$-**1**, and its two components are generated from the fundamental configuration of $^6\Sigma^+$ by single electron shifts from π_{xz} to π_{yz} and vice versa. Based on Table 5, the $d_{xz}-d_{yz}$ relationship generates a *z* component of the SOC. Similarly, the p_x, p_y AO's on the oxygen generate a *z* component of the angular momentum.[9] A second fundamental configuration which contributes to $^4\Sigma^-$ is shown in Scheme 2 as $^4A_2$-**2**. This configuration has a smaller coefficient in the MCSCF wave function, but its intrinsic SOC matrix element with the sextet configuration is large due to the $d_{xy} - d_{x^2-y^2}$ relationship (Table 5). Together, the two matrix elements, in eqs 17a and 17b, contribute to the significant *z* component of SOC in Table 1.

$$\langle {}^6A_1({}^6\Sigma^+)|\mathbf{H}_{SO}|{}^4A_2\text{-}\mathbf{1}({}^4\Sigma^-)\rangle_z = 0.5(c^2{}_{Fe}\zeta_{Fe} + c^2{}_O\zeta_O) \quad (17a)$$

$$\langle {}^6A_1({}^6\Sigma^+)|\mathbf{H}_{SO}|{}^4A_2\text{-}\mathbf{2}({}^4\Sigma^-)\rangle_z = \zeta_{Fe} \quad (17b)$$

The above examples demonstrate that the angular momentum and symmetry selection rules are not redundant, but lead to complementary insight.

(b) Orbital Effects on SOC in FeO^+-H_2 Structures. The interaction of FeO^+ with H_2 is attended by orbital delocalization and increased MCSCF mixing, especially for the quartet states of ^4C_R and ^{4}TS. The corresponding sextet state is still dominated by a single open-shell configuration ($c \geq 0.6$) akin to the $^6\Sigma^+$ parent configuration of FeO^+. This fundamental configuration is shown in Scheme 3 (**1**−**3**) for the C_R and TS species.

Relying on these configurations, the SOC patterns (refer to Table 2) can be related to their FeO^+ ancestry. As indicated in **4** in Scheme 3, the $^4B_2$ configurations of C_R are generated from the $^6A_1$ configuration by shifting an electron from $2\pi_{xz}$ to δ_{xy}, and contributing thereby an *x* component of SOC,[26] much like the FeO^+ case discussed in eq 13a. Similarly, shifting an electron from $2\pi_{xz}$ to $\delta_{x^2-y^2}$ generates the $^4B_1$ state, leading thereby to a *y* component of SOC as in the FeO^+ case in eq 15b. Finally, an electron shift from $2\pi_{xz}$ to $2\pi_{yz}$ as well as from 3σ to δ_{xy} generates the $^4A_2$ state. Since the 3σ orbital in ^6C_R is a hybrid with a $d_{x^2-y^2}$ character (and d_{z^2} of course), the latter electron shift involves an angular momentum term, $\langle d_{xy}|l_z|d_{x^2-y^2}\rangle$. These orbital factors are responsible therefore for generating a *z* component of SOC, by analogy to the situation in FeO^+ described in eqs 17a and 17b.

In the ^4C_R cluster (note the change in axes), **2** in Scheme 3, the major $^4A''$ configurations (**5**) are generated from the fundamental sextet configurations, $^6A'$, by shifting electrons from $2\pi_{xy}(a')$ to $\delta_{yz}(a'')$ and from 3σ to $\delta_{yz}(a'')$. These two shifts are responsible for the *x* and *y* components of the SOC, by analogy to the $^4B_{1,2}$ states in FeO^+.

The fundamental $^6A'$ configuration for the two TS's is shown in **3** in Scheme 3. Electron shifts, either from $\delta_{xz}(a'')$ to 3σ or from 3σ to $2\pi_{yz}(a'')$ and vice versa (**6**), generate the $^4A''$ configurations and lead to *x* and *y* components of the SOC.

(c) Variations in the Value of the SOC Matrix Element Along the Reaction Path. The final feature of the calculation that requires understanding is the variation of the SOC matrix element along the reaction pathway. Recalling that the states are MCSCF wave functions, eqs 4a and 4b, we can express the total SOC matrix element (in absolute magnitude) for a component *r* in eq 18,

(26) The secondary configurations involve excitations from the bonding MO's to the nonbonding ones. The SOC matrix elements between the secondary configurations mimic those between the main configurations.

Scheme 3

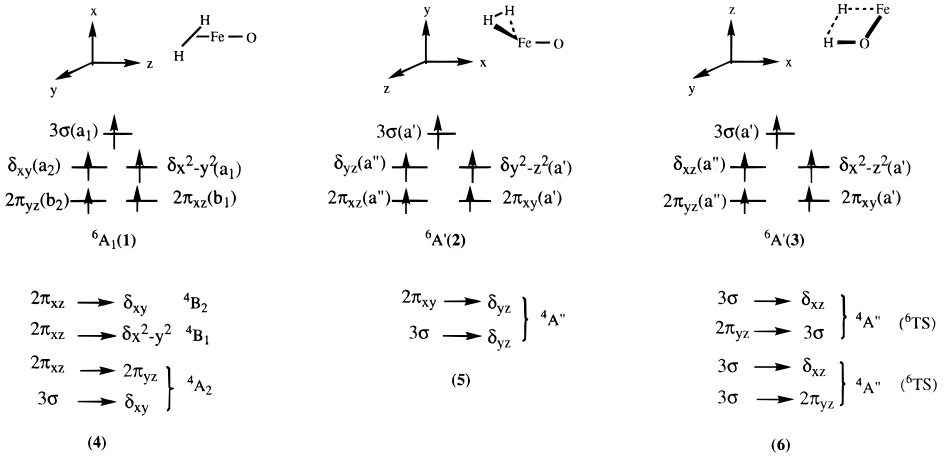

$$|[\langle \mathbf{H}_{SO}\rangle_r]_{1,2}| = 0.5\sum_{I;J} W_{Ik,Jk'} c_I c_J \sum_K \zeta_K \langle \varphi_\mu | l_{rK} | \varphi_\nu \rangle \quad (18)$$

where we have already considered the nonvanishing spin factor (0.5). The $W_{Ik,Jk}$ term is the Ms-dependent weighing factor (eq 12d). In the present case, where state 1 is the sextet, the fundamental open-shell configuration has one dominant coefficient. To simplify we assume a single sextet configuration with coefficient $c_I = c_0$.

The MO's in the angular momentum expectation values, in eq 18, above involve in principle contributions from Fe, O, and H, as in eq 19.[10a]

$$\varphi_\mu = c_{Fe}\mathrm{d}_{rs} + c_O\mathrm{p}_r + c_H\mathrm{1s}; \qquad \varphi_\nu = c'_{Fe}\mathrm{d}_{rs} + c'_O\mathrm{p}_r + c'_H\mathrm{1s} \quad (19)$$

Since the 1s orbital of H does not contribute to the angular momentum expectation value, the final SOC expression becomes eq 20. Here, the m_d parameters are the coefficients of the angular momentum expectation values in Table 5, while the cc' factors are products of the MO coefficients in eq 19 for a given atom.

$$|[\langle \mathbf{H}_{SO}\rangle_r]_{1,2}| = 0.5c_0\sum_J W_{0k,Jk'} c_J [m_d(cc')_{Fe}\zeta_{Fe} + (cc')_O\zeta_O]; \quad m_d = 1, \sqrt{3}, \text{ or } 2 \quad (20)$$

Equations 19 and 20 provide a basis for understanding the variation of SOC along the reaction pathway. Whenever one or both MO's, eq 19, are pure d orbitals, the $(cc')_O$ product in eq 20 vanishes. In all other cases, the oxygen terms contribute to the SOC matrix element, but to a lesser extent than the iron due to the ratio of the atomic constants ζ_{Fe}/ζ_O of ∼3. Thus, to a rough approximation, the SOC matrix element is dominated by the iron-centered terms, and as such will be determined by the variation of two main factors: (a) the delocalization of the MO's as accounted for by the $(cc')_{Fe}$ MO coefficient term, and (b) the MCSCF coefficient, c_J, of the quartet substate. The more extensive the orbital mixing between the FeO^+ and H_2 moiety, the smaller the coefficient on the Fe gets. Similarly, the more extensive the orbital mixing, the more correlated the quartet wave function becomes, and as such its individual MCSCF coefficients, c_J, become smaller. Since the number of configurations which differ from the fundamental sextet configuration by single electron shifts is fixed, the increased delocalization of the MCSCF wave function means necessarily a smaller SOC matrix element in eq 20.

At the reactant entrance of Figure 1, FeO^+ has a sextet state described by a dominant configuration ($c_0 = 0.75$), and a quartet state dominated by a single configuration ($c_J = 0.5$). As such, FeO^+ possesses significant SOC matrix elements, given by the coefficient-weighted atomic constant of Fe^+ (see eq 16: $c_{Fe}\zeta_{Fe}$); the largest of the matrix elements is ∼50% of the atomic constants (407−416 cm^{-1}). At the ^6C_R cluster geometry, there occurs some orbital mixing with H_2, accompanied by increased configuration mixing. Thus, the coefficients (eq 20) c_0, c_J, and c_{Fe} all decrease, and the SOC matrix element is decreased further reaching at most 30% of the Fe^+ atomic constant. At the ^4C_R geometry where the mixing continues to increase, the SOC matrix element further decreases. This trend goes on at the TS geometries where the bond making and breaking becomes extensive. The lowest SOC value reaches 4−15% of the atomic constant at the ^{6}TS geometry which involves the highest degree of bond distortion (Scheme 1). Our analysis suggests that the trend will peak at the geometries of the insertion products, $^{4,6}I$ (Figure 1), where the H_2 molecule adds to FeO^+ and forms two new bonds Fe−H and O−H, both of which are expected to delocalize the orbitals and decrease the contributions of the Fe and O atoms to the SOC matrix elements.

Starting with the insertion intermediate, H_2O elimination begins and the orbitals get increasingly less delocalized until they eventually localize on the Fe^+ and H_2O fragments. Nevertheless, Table 3 shows that the SOC between the sextet ground state and the lowest quartet state of the C_P cluster are small or virtually zero (entries 1,2 and 5,6). To understand the reason, we need to consider the effective states which describe the Fe^+ moiety within the cluster. For the sextet ground state of the cluster, $^6A_{1,2}$, the Fe^+ moiety is basically in a $4s^13d^6$ situation, as in the ground state of free Fe^+, while for the quartet state, $^4A_{1,2}$, the constituent of the Fe^+ moiety is some mixture of the $^4F(3d^7)$ and $^4D(4s^13d^6)$ states.[24]

Consider first the realistic situation where the major atomic constituent of Fe^+ in ^4C_P is the ^{4}F-like ($3d^7$). In this case, the $^6C_P-{}^4C_P$ SOC will resemble the $^6D(4s^13d^6)-{}^4F(3d^7)$ SOC in the atomic state. These terms arise from a shift of an electron from a 4s to a 3d orbital, and hence contribute zero SOC, as is indeed reflected from entries 5 and 6 in Tables 3 and 4. Accordingly, we expect a very small SOC at the SI junction corresponding to $^6C_P-{}^4C_P$ intersection.

Consider now the situation, which is encountered in our computations, and in which the dominant Fe^+ constituents in ^4C_P are ^4D-$4s^13d^6$ types. In this case, the $^6C_P-{}^4C_P$ SOC should resemble the $^6D-{}^4D$ SOC in the atomic state. Comparison of the SOC terms in the cluster with the atomic ones ($^6A_{1,2}-{}^4A_{1,2}$

in entries 1,2 in Table 3 with the same entries in Table 4) shows the anticipated similarity in the SOC values. Note that even though the ^{6}D−^{4}D SOC is not zero, it is nevertheless only 20% of the atomic constant, a fact that traces to the common $4s^13d^6$ electronic structure of ^{6}D and ^{4}D, due to the many determinants required to describe the low-spin situation. Thus, the resulting ^{6}D−^{4}D SOC matrix element will involve a sum of terms weighted by small weighing factors (eq 20), and which occur in opposite signs (as verified by us for $^6A_{1,2}$−$^4A_{1,2}$), leading thereby to small SOC.

In summary, since the calculations of Rossi et al.[24] show that the ^{4}F term dominates the quartet states of $Fe^+\cdots OH_2$, the SOC matrix elements should be very small, thus closer to the values in entries 5 and 6 in Table 3. Past the cluster, the sextet−quartet SOC in Fe^+ involves the state pair ^{6}D−^{4}F and the SOC matrix elements and will be virtually zero, as in entries 5 and 6 in Table 4.

(d) Spin Inversion Probabilities for the Reaction. The essence of the above discussion is pictured in Scheme 4, which uses the variation of the maximal SOC matrix element along the reaction pathway. Thus, the SOC matrix element between the sextet and quartet states is largest at the FeO^+ reactant, and decreases gradually toward the Fe^+ product channel. Since the sextet and quartet states of FeO^+ are well-separated,[22] the first SI junction which is available for spin flip and formation of the quartet insertion intermediate, ^{4}I, occurs only later; somewhere in the region of the clusters and TS's of the insertion step (Figure 1). A second SI junction occurs at the onset of the elimination step near the ^6C_P cluster. As seen from Scheme 4, the sextet−quartet SOC matrix elements in the potentially available second SI region are quite small. Thus already at the outset it is clear that the probabilities for crossover at the SI junctions cannot be large, and will therefore hamper the efficiency of the bond activation process.

A crude estimate of these probabilities is possible using the Landau−Zener[27] treatment, which is often employed for similar purposes.[10i−l] Even the Landau−Zener treatment cannot be anything but an approximately qualitative one due to various factors as detailed below. As such, we shall not dwell on the numerical values, but aim to derive insight and qualitative trends.

The Landau−Zener equations for the probability of single (P') and double (P'') passes through the SI junction are shown in eqs 21a and 21b.

$$P'_{12} = 1 - y; \quad y = \exp\{-4\pi^2(\mathrm{SOC})^2/h\upsilon|F_1 - F_2|\} \quad (21a)$$

$$P''_{12} = 2y(1 - y) \quad (21b)$$

Here, SOC is the matrix element between the two spin situations, υ is the effective velocity of passing through the crossing point, and the $|F_1 - F_2|$ term is the difference in the slopes of the two intersecting surfaces at the crossing point.

The SI region for the bond insertion step is in between the clusters and the transition states. Without an accurate location of the crossing point (energies are at the CASPT2 level[2e]), it is reasonable to look at the matrix elements for all these species as though they represent the matrix element at crossing points. Since the states within the sextet and quartet manifolds are generally well-separated near the SI junction of bond insertion, we can use for each spin situation a single spatial state. Assuming that the substates of a given spin situation are thermally averaged, then the effective SOC matrix element between two states is the root-mean square of the sum of matrix

Scheme 4

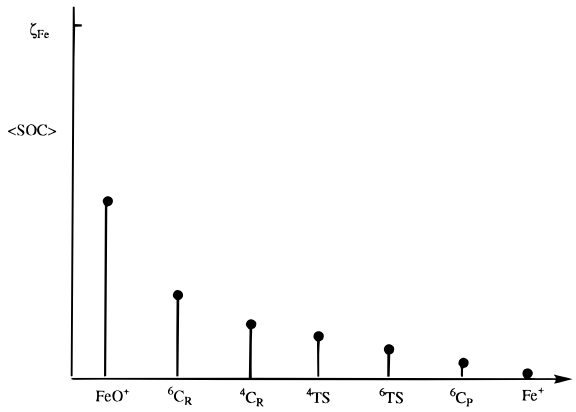

elements over substates (k, k'), and over the x,y,z components of the SOC operator. All these are divided by the statistical factors,[9b] as shown in eq 22. Thus, eq 22 will not allow us to consider substate specificity although such effects may be anticipated from the matrix elements in Table 2.

$$\mathrm{SOC}_{1,2} = \{[1/(2S_1 + 1)(2S_2 + 1)][\sum_{k,k'}(\langle \mathbf{H}_{\mathrm{SO}}\rangle_{k,k'})_x^2 + \langle \mathbf{H}_{\mathrm{SO}}\rangle_{k,k'})_y^2 + (\langle \mathbf{H}_{\mathrm{SO}}\rangle_{k,k'})_z^2\}^{1/2} \quad (22)$$

Since the crossing point is not available, the slopes of the two states have to be approximated. A large slope difference is expected, since both experiment[2a,c,d] and theory[2e] show that the sextet state rises steeply from the ^6C_R cluster toward the ^{6}TS, while the quartet state has a flat surface between the respective quartet species. Using the CASPT2 energies of the Berlin group[2e] and considering that the effective coordinate that leads to the bond insertion TS's is the H- - -H stretch coordinate, we obtain a slope difference of 89.4 kcal/(mol Å). Calibration of the sextet and quartet barriers[28] by the experimentally estimated ones leads to a slope difference of 72.34 kcal/(mol Å). To be on the safer side, we also have used lower values of down to 10 kcal/(mol Å). The relative velocity of the two reactants is evaluated from the sum of translational energies of the two reactants at 300 K. All these estimates will give us a range of probabilities, not necessarily a drawback considering the qualitative nature of the treatment.

Using eq 22 to calculate the effective SOC interactions between the sextet and quartet states leads to values (in cm^{-1}) of 69, 41, 33, and 39 for the geometries defined by the ^6C_R, ^4C_R, ^{6}TS, and ^{4}TS species. Since the probabilities vary in proportion to the square of the matrix element, the highest probability is obtained assuming a crossing point near the ^6C_R species, while the smallest probability occurs near the ^{6}TS species. Taking an average of these matrix elements along with the slope difference of 72.34 kcal/(mol Å) leads to average passage probabilities of 4.3×10^{-3} for a single pass and 8.4×10^{-3} for a double pass, while for a slope difference of 20 kcal/(mol Å), the corresponding probabilities were 1.52×10^{-2} to 3.0×10^{-2}. Further decrease of the slope difference to 10 kcal/(mol Å) changes the average probabilities to 3.0 ×

(27) Zener, C. *Proc. R. Soc. London, Ser. A* **1932**, *137*, 595; **1933**, *140*, 1174.

(28) At the CASPT2//DFT level used in ref 2e the quartet state's energies for FeO^+ are overestimated relative to the sextet states by ca. 7 kcal/mol. Applying this factor to all the quartet surface in ref 2e gives an energy of −1 kcal/mol for the ^{4}TS relative to the reactant onset in Figure 1 here.

(29) For stability trends in Fe^+/RH clusters see ref 1.

(30) Ryan, M. F.; Fiedler, A.; Schröder, D.; Schwarz, H. *J. Am. Chem. Soc.* **1995**, *117*, 2033.

(31) Dillinger, B.; Hochstrasser, R. M.; Smith, B. A., III *J. Am. Chem. Soc.* **1977**, *99*, 5834.

(32) Leung, M.; El-Sayed, M. A. *J. Am. Chem. Soc.* **1975**, *97*, 669.

10^{-2} to 5.9×10^{-2} and does not affect the ballpark figures of low probabilities in the range of 6×10^{-2} to 4×10^{-3}. Using the highest single SOC matrix element between the sextet substate with Ms = $^5/_2$ and the quartet substate with Ms = $^3/_2$ (Table 2, entry 1) leads to higher probabilities of the order of 0.11−0.46.

The range of SI probabilities we generated is not low enough to rule out the effect of energetic or entropic factors on the observed sluggish efficiencies of the reaction. Nevertheless, the calculations show that the SI factor will have a significant influence on the efficiency of bond activation. The probability of SI is sensitive to the SOC matrix element, and the highest probability in the SI region is nearer to the ^6C_R cluster or even closer to the reactant end, FeO^+, provided an SI junction can be achieved there.

The second SI junction in Figure 1 occurs en route to the ^6C_P cluster. Since the $^6A_{1,2}-^4A_{1,2}$ state separation is small (see footnote 58 in ref 2c), the SI junction is possibly very near the cluster. As argued above our calculated SOC matrix elements for this cluster (entries 5, 6 in Table 3) are very small. Even the single largest matrix element in Table 3 does not predict a probability higher than $\sim 10^{-2}$ for the passage from the insertion intermediate to the ^6C_P cluster.

(e) Correlation of an SI-Controlled Scenario with Experimental Data. Since the experimental data[2c,d] as well as the computational data[2e,3] suggest that the ^{4}TS on the quartet surface is likely to be below the energy asymptote of the reactants,[28] a reasonable approach would be to assume a SI-controlled reactivity and to try and examine this assumption in the light of the experimental data.

Let us commence with the bond insertion step and make reference to the species in Figure 1. The FTICR study of the Berlin group[2a] shows that a thermalized FeO^+ generates only Fe^+ (presumably also H_2O), as required by the limiting exothermicity factor under thermalized conditions. The observed rate constant of 1.6×10^{-11} cm^3/(s molecule) is slightly higher than the one measured by the Utah group,[2c] 1.5×10^{-12} cm^3/(s molecule), both being two to three orders of magnitude lower than the collision rate constant ($k_L = 1.6 \times 10^{-9}$ cm^3/(s molecule),[33] and could be accounted for by using the lower end of our SI probabilities. This does not rule out, however, a SI-controlled situation with a contribution of other kinetic bottlenecks. The observation of the Berlin group[2a,33] that the reactions of $FeO^+/H_2(D_2)$ exhibit virtually no kinetic isotope effect (KIE) may originate in the effect of increased lifetime of the FeO^+- - -D_2 cluster in comparison with its hydrogen isotopomer which offsets the KIE.[2a] However, an alternative explanation is that the lack of KIE reflects in fact an SI-controlled process which is not affected by isotopic substitution. With kinetically excited FeO^+, both groups observed an initial decrease of the reaction efficiency, followed by an increase of the efficiency as the kinetic energy increases.[2a,c] This behavior was ascribed to a barrier on the sextet surface. The experimentally determined[2c,d] value of the barrier is 0.6−0.75 eV above the reactants, in reasonable accord with the computational results of the Berlin group in Figure 1 (see ^{6}TS in Figure 1).[2e] Thus, at low kinetic energy the reaction is constrained to pass through the SI junction, and the efficiency decreases as the relative kinetic energy of the reactants increases in accord with a nonadiabatic SI-controlled process. At higher excitation energies the system has sufficient energy to pass along the sextet surface, cross the barrier (^{6}TS), and slide to the sextet product cluster (^6C_P) in a spin-conserving manner. This is precisely the scenario deduced by the Utah group.[2c,d] Thus, the experimental trends follow a SI-controlled scenario, albeit alternative explanations do exist.

The assumption of a SI-controlled bond insertion step enables us to make some verifiable predictions. Thus, as long as the SI junction for the bond insertion step is located in the region between the clusters, C_R, and the transition states, TS's, the probability for crossover will be low. Any factor which shifts the SI junction closer to the FeO^+ reactant will increase the probability of crossing from the sextet surface to the quartet bond insertion intermediate, and hence will improve the efficiency of bond activation. One obvious factor that controls the location of the SI junction is the stability of ^4C_R, the quartet cluster. It is anticipated then that as the cluster's stability increases, the SI junction will move to an earlier position and be closer to the FeO^+ reactant limit where SOC is significant, resulting thereby in improved reaction efficiency.

Table 7 shows some data taken from a recent review by the Berlin group.[1] It is seen that the reaction efficiency for FeO^+ activation reactions changes from 1% with H_2 to 20, 50, and 100% with alkanes C_nH_{2n+2} ($n = 1-3$) of increasing size. This increase of efficiency correlates with the stability of the FeO^+- - -RH quartet cluster.[2e,3,29] The same correlation is observed for CoO^+ and NiO^+.[1,2d] While this increase of reactivity may be ascribed to the increased lifetime of the clusters, a plausible alternative is that this is an outcome of shifting the SI junction closer to the reactant end where the SOC factors are larger. The lifetime factor may well assist the crossing of the SI junction by allowing many passes within the lifetimes of the $^{4,6}C_R$ clusters.

Table 7. Reaction Efficiencies (Φ) and Relative Yields of Products[a]

		% yield	
reactants	Φ (%)	MOH^+/H(R)	M^+/ROH(HOH)
1. FeO^+/H_2	1	0	100
2. FeO^+/CH_4	20	57	41
3. FeO^+/C_2H_6	50		
4. FeO^+/C_3H_8	100		
5. CoO^+/CH_4	0.5		100
6. NiO^+/CH_4	20		100
7. MnO^+/CH_4	40	100	<1
8. MnO^+/H_2	15	75	25

[a] Data from ref 1.

Consider now the product channel, where the SOC terms reach their minimum. Starting from Fe^+ and D_2O, Armentrout et al.[2c] showed that the ^{4}F excited state of Fe^+ leads to a more efficient reaction than the ^{6}D ground state by a factor of 200. Furthermore, FeO^+ could not be observed among the products even though products of higher endothermicity were generated. These findings accord with the SOC results, that the very small sextet−quartet SOC at the $^6C_P-^4C_P$ SI junction (Figure 1) does not permit the interconversion of the different spin situations. The results lend support to Armentrout's conclusion,[2c] that the peculiar behavior reaction of Fe^+ with H_2O (D_2O) is due to extremely inefficient ^{6}D−^{4}F mixing, and show that this poor SOC is rooted in the electronic structures. Thus, since the one-electron shift, from $4s^13d^6$ for ^{6}D to $3d^7$ for ^{4}F, is of the s → d type, the respective SOC is zero.

The most diagnostic role of the SI junction is at the M^+ exit channel, where differences in the product distributions can be expected for cases where M^+ has a $4s^13d^n$ ground state (Fe^+, Mn^+), in comparison with cases where M^+ has a $3d^n$ ground state (Ni^+, Co^+).[1] This difference is best illustrated in the reactions of $MnO^+(^5\Sigma^+,^5\Pi)$ that undergoes a spin-conserving

(33) Schröder, D.; Schwarz, H.; Clemmer, D. E.; Chen, Y.; Armentrout, P. B.; Baranov, V. I.; Bohme, D. K. *Int. J. Mass Spectrom. Ion Process* In press.

bond insertion[30] but must cross an SI junction at the exit channel[3] to produce Mn^+ (^7S) and ROH. Entries 7 and 8 in Table 7 show that while MnO^+ is an efficient activator, in accord with its spin conserving bond insertion step, it gives very small yields of H_2O and CH_3OH, in accord with the expected small SOC terms between the high- and low-spin states of the Mn^+- - -ROH cluster at the exit channel. Thus, the MnO^+/RH system bypasses the SI junction and gives rise to the $MnOH^+$/$R^\bullet$ product which is spin conserving.[3,30] In contrast, CoO^+ and NiO^+, which possess a SI junction for bond insertion, do not have to invert spin at the elimination step because the ground state of the corresponding metal ions is $3d^n$. Indeed, entries 5 and 6 in Table 7 show that CoO^+ and NiO^+ undergo inefficient bond activation (low overall efficiency), but nevertheless produce only the M^+/ROH products. As may be seen from entry 2, the reaction of FeO^+ with CH_4 is quite efficient, but nevertheless, the yield of Fe^+/CH_3OH is only 41%, in good analogy with the MnO^+/RH cases.

Concluding Remarks

The process $FeO^+ + H_2 \rightarrow Fe^+ + H_2O$ (eq 1) involves two spin inversion (SI) junctions between sextet and quartet states: near the FeO^+/H_2 cluster at the entrance channel, and near the Fe^+/H_2O cluster at the exit channel. *Due to the large barrier (≥18 kcal/mol) on the sextet surface, the only potential for bond activation is the crossover to the quartet surface which affords a low-energy path for the bond activation. As such, the overall reaction efficiency is limited by the SOC between the two spin states at the SI junctions.*

An important requirement for SOC is that the two spin states must differ by a shift of an electron between two iron orbitals, none of which is an s orbital, which differ by their mutual orientations (Tables 5 and 6). Using this guideline, it is anticipated and corroborated by computations that the SOC will be gradually reduced from its initial value at the reactant extreme (for FeO^+), due to orbital mixing and delocalization of the iron orbitals during the bond insertion step. At the elimination step which starts with the Fe^+- - -OH_2 cluster, the SOC terms are small and should diminish to virtually zero for the ^6D and ^4F states of Fe^+, due to the fact that their electronic structures are $4s^13d^6$ and $3d^7$, respectively. It follows, therefore, that the electronic structure of the spin states down sizes the SOC matrix elements, *and even though Fe^+ has a large SOC constant, this does not carry over to the SOC between the sextet and quartet states along the oxidation process*.

Assuming that the overall process is dominated by the SI junctions forms a basis for understanding the experimental findings of Schwarz et al.[1,2a,e,30] and Armentrout et al.,[2c,d] and for verifying their basic conclusions.[33] Based on the understanding of the SOC patterns, predictions are made for analogous processes, $MO^+ + RH \rightarrow M^+ + ROH$ (M = Mn, Fe, Co, Ni; R = H, alkyl), and compared with appropriate experimental data.[1,2]

Our SOC computations as well as the selection rules suggest that both reactivity and product distribution should be substate selective. The fact that such selectivity is observed among the spin substates of triplet states of organic molecules[31,32] suggests that such a selectivity may play a role in the reactions of transition metal species.

Clearly an assumption of an SI-controlled process is a gross oversimplification, and a proper treatment of the dynamics of the process is required. Nevertheless, the kinetic role of the SI junction appears evident, and should form an incentive for further investigation of the effects of spin inversion in analogous systems.

Acknowledgment. Some of this research was carried out during a sojourn of S.S. in the University of Rochester. S.S. thanks J. P. Dinnocenzo for kind hospitality during the visit to Rochester. The research was supported in part by a Grant from the G.I.F., The German−Israeli Foundation of Scientific Research and Development, and in part by the Volkswagen Stiftung.

JA963033G